FEDERAL UNIVERSITY OF ITAJUBA
GRADUATE PROGRAM
IN ELECTRICAL ENGINEERING

OPERATION AND RESTORATION OF BULK POWER SYSTEMS USING DISTRIBUTED ENERGY RESOURCES AND MULTI-MICROGRIDS

Maíra Ribas Monteiro

Itajubá,
July 2021

FEDERAL UNIVERSITY OF ITAJUBA
GRADUATE PROGRAM
IN ELECTRICAL ENGINEERING

Maíra Ribas Monteiro

Operation and Restoration of Bulk Power Systems Using Distributed
Energy Resources and Multi-Microgrids

July 2021
Itajubá – MG

FEDERAL UNIVERSITY OF ITAJUBA
GRADUATE PROGRAM
IN ELECTRICAL ENGINEERING

Maíra Ribas Monteiro

Operation and Restoration of Bulk Power Systems Using Distributed Energy Resources and Multi-Microgrids

The following individuals certify that they have read and recommended this thesis to the Graduate Program in Electrical Engineering for acceptance, in partial fulfillment of the requirements of the degree of Doctor of Philosophy.

Committee members:

Dr. Antonio Carlos Zambroni de Souza, ISEE, UNIFEI

Supervisor

Dr. Benedito Donizeti Bonatto, ISEE, UNIFEI

Supervisory Committee Member

Dr. Eliane Valença Nascimento de Lorenci, ISEE, UNIFEI

Supervisory Committee Member

Dr. João Guilherme Carvalho Costa, ISEE, UNIFEI

Supervisory Committee Member

Dr. Ahda Pionkoski Grilo Pavani, CECS, UFABC

External Examiner

Dr. Walmir de Freitas Filho, DSE, UNICAMP

External Examiner

Itajubá

2021

To my parents,

Maria Inés and Luiz Carlos.

Acknowledgments

First, I would like to thank God for His guidance and blessing in developing this work and my professional and personal growth in face of different challenges. I humbly ask for wisdom to continue my journey.

I would like to express my special gratitude to my supervisor, Dr. Antonio Carlos Zambroni de Souza, for his continued guidance, support, and encouragement to take the next step at different stages throughout my Ph.D. development at UNIFEI and The University of British Columbia (UBC). My gratitude is also extended to Dr. Liwei Wang and Dr. Morad Abdelaziz for their support during my stay at UBC. In addition, I would like to thank my Ph.D. committee members, Dr. Benedito D. Bonatto, Dr. Eliane V. N. de Lorenci, Dr. João Guilherme C. Costa, Dr. Ahda P. G. Pavani and Dr. Walmir de Freitas Filho, for accepting to referee this thesis.

I would like to deeply thank my parents, Mr. Luiz Carlos Monteiro and Mrs. Maria Inês O. R. Monteiro, who always worked without measuring efforts to bring me where I am, and for being my foundation and providing unconditional support and love, even if it was required to be far away for a long time. To my sister and brother, Dr. Juliana R. Monteiro and M.Sc. Luiz Fernando R. Monteiro, who always encouraged me to move forward to achieve my goals and I am so proud to have you in my life.

Also, I would like to thank my husband, future Dr. Yuri R. Rodrigues, for his endless support, love, encouragement and for being by my side. You are so important to me, and I am so grateful to be able to share my experiences and life with you. Still, I wish to thank my family, friends and everyone involved in this period of my life.

Abstract

The fast-paced and meaningful penetration of distributed energy resources (DERs), such as variable renewable energy sources (RESs), concurrently with the widespread occurrence of natural disasters and man-made threats, has raised several challenges for the modern bulk power systems (BPSs) status quo. Although the DERs are demanding new solutions to ensure adequate stability and security levels, these resources enable significant opportunities to improve multiple BPS perspectives. In this view, seeking to capitalize on these novel features, while aware of the significant changes to BPS outlook, this thesis is focused on developing new methods able to capitalize on modern monitoring infrastructures, DERs and control areas opportunities toward the improvement of BPS operation and stability.

Specifically, the thesis focuses on: 1) First, a novel method for the improvement of the static security region (SSR) is proposed based on a new network partitioning algorithm. The proposed algorithm focuses on modern BPS with high penetration of variable RES generation. It divides the BPS into coherence areas according to its criticality mapping, and consequently, areas are adaptively associated with SSRs generators groups. To this end, each bus is assigned a criticality index from the potential energy function, whereas this calculation is based on the data of the wide-area measurement system (WAMS) using phasor measurement unit (PMU); 2) Second, a novel area-based sensitivity index for voltage stability support is proposed, exploring both the network-wide sensitivity and the local characteristics of voltage collapse. The developed index focuses on the determination of the most effective buses for voltage support and their respective capability of increasing the system's load margin. For this, a novel area-based outlook is developed taking advantage of the new possibilities enabled by BPS distributed controllable resources, such as flexible resources (FRs).

Keywords: Bulk power system, distributed energy resources, network partitioning, static security region, voltage stability

List of Figures

List of Tables

Table of Contents

Chapter 1:   Introduction

1.1 Context

In Chapter 1, the motivation of this research work to develop new solutions for the operation and stability of modern bulk power systems (BPS) is presented. Thereafter, background information and literature survey are presented to contextualize the research tasks. Finally, the research objectives and the thesis layout are defined.

1.2   Motivation

Growing concerns about climate changes and electricity demand have motivated modern BPS to move towards a significant increase in distributed energy resources (DERs) penetration. These resources can accelerate and provide significant and needed improvements to the operation and planning of BPS. Although these resources have meaningfully advanced support services, their integration presents challenges that compromise multiple BPS technical outlooks, including stability, operation, and restoration capacities. In addition, large-scale renewable energy sources (RESs) are already being deployed as an efficient pathway to reduce current greenhouse gas emissions, however, these sources are variable and intermittent, and consequently, they impact the voltage and frequency performance of BPS.

As the BPS operation undergoes several operational scenarios that present different penetration levels of RES generation, the intermittence of these sources significantly influences the coherence areas, i.e., parcels of the system that possess a similar behavior. As a result, changes in the set of buses comprised in each coherence area must be considered. Simultaneously, the generator groups for the traditional construction of static security regions (SSRs) are kept fixed throughout the system operation. In this perspective, control actions can become ineffective or even lead to undesirable consequences, e.g., voltage collapse [1], with the consideration of invariable generator groups. Consequently, the SSRs' inability to track the changes of coherence areas drives to a significant narrowing in the system's security, reducing the operator's ability to maneuver the system and maintain its stability margin. This characteristic increases the system's susceptibility to instability in case of unexpected events.

To cope with this perspective, advances in BPS monitoring can provide a precise perspective of the system operating conditions.

Additionally, ensuring a safe voltage stability margin is a critical aspect of BPS reliability [2]. Traditionally, the required voltage stability margins had been achieved using VAR compensating devices, e.g., static VAR compensators (SVC) [3]. These components are typically allocated at the network's most critical buses as identified by system-wide sensitivity analysis [4]. However, this can lead to overcompensation in specific system regions as the identified critical buses tend to be close to each other [4]. Moreover, as BPSs move towards an increased penetration of RESs, these approaches may no longer be efficient, since the variable and uncertain generation of such sources can significantly affect the system static stability margins [3],[5] and can continuously move the starting point of voltage collapse across different regions of the system. On another avenue, recent developments in monitoring and control have been leading to a pronounced improvement in power system flexible resources (FRs) capacity [6], including the use of energy storage systems (ESS), distributed generation (DG), electric vehicles (EVs) and demand response (DR) to provide load flexibility.

Overall, this thesis seeks to overcome current issues that limit the full performance of modern BPS with high penetration of DERs. To this end, this thesis is focused on evaluating and harnessing new opportunities enabled by modern BPS, including advanced monitoring and DERs. Its contributions include three distinct yet correlated perspectives that can meaningfully improve the operation, stability and restoration of modern BPS in face of the increasing integration of DERs.

1.3   Background

1.3.1 Distributed Energy Resources

DERs are defined are composed of distributed generation, energy storage, and/or controllable loads connected to DS. These resources allow the development of effective solutions capable of significantly increasing the flexibility of BPS. Along with the advent of BPS modernization, the increasing penetration of DERs has motivated the transition from traditional DS towards active DS (ADS) and MG, as represented in Figure 1.1.

However, the integration of these resources in modern BPS presents meaningful challenges to ensure efficient BPS operation, stability, and restoration processes, including aspects such as unpredictable power, low inertia, demand forecast error, frequency, and voltage instability. Yet, regardless of these challenges, DERs are considered worldwide as an important part of BPS modernization toward clean energy supply and reliability services [16]. To ensure that the benefits of DER can be fully realized, an adequate definition of control areas is fundamental.
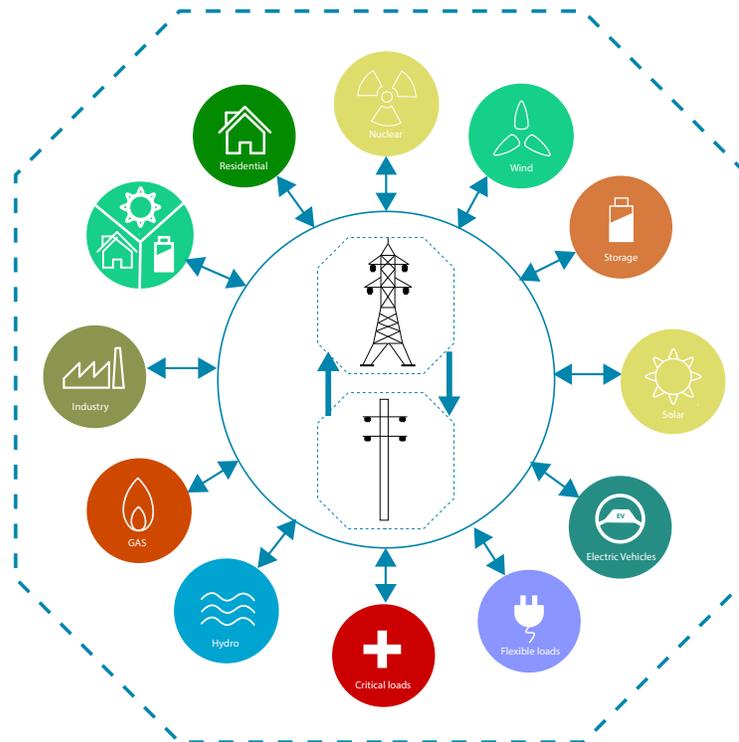
Figure 1.1: Modern bulk power system

1.4 Literature Review

In this section, the literature review focuses on network partitioning and voltage stability of BPS to contextualize the proposed research tasks with the state-of-art.

1.4.1 BPS Network Partitioning

Several approaches have been proposed in the literature. In [31], methods based on network partitioning, as of right eigenvector and tangent vector, are used to speed up the computation of voltage collapse points. The grid partitioning for parallel power system restoration is employed in [17]. In [18] a partitioning strategy for volt/VAR control is performed by spectral graph clustering. Secondary voltage control-driven approaches are proposed in [19], based on a graph partitioning method, and [20] uses two decomposition methods considering the network electrical distances. The concept of the voltage control areas (VCAs) is employed in [21] using unsupervised (k-means) and supervised (support vector machines) learning techniques for the identification of voltage stability weak areas. A hybrid method combining conventional and evolutionary graphs seeking to optimize a multi-attribute objective function is presented in [22]. In [32] a novel Laplacian spectrum-based approach to directly solve partitioning problems considering the context of smart grids is proposed. A partitioning method using the Koopman mode analysis (KMA) is depicted in [33]. Further, network partitioning methods seeking the adequate placement of phasor measurement units (PMU) for dynamic vulnerability assessment are depicted in [34]-[35]. Still, there is a gap in network partitioning methods that employ the new situation awareness provided by wide-area measurement system (WAMS) using PMUs to track power systems coherence areas variation. Moreover, there is still a need for a method to adaptively determine the generator groups for the improvement of SSRs for BPS with large penetration of RESs.

1.4.2 BPS Security Regions

The increasing participation of RESs presents significant challenges in ensuring BPS operation within the adequate security and reliability standards, especially due to their intermittence. These sources can meaningfully impact SSR definition [36]-[37], i.e., in a multi-dimensional space mapping of the operating points that ensure the system operates within technical limits, such as under- and over-voltage, thermal, and maximum active power generation [38]-[39]. Due to its major importance, several techniques have been investigated in the literature to improve BPS static security. An algorithm to construct inner approximations of static security is developed in [36]. The maximal static security region is proposed in [40]-[41]. A new stochastic optimal power flow considering the static security constraints is presented in

[42]. In [43] the distance to the boundaries of the security region is used for its construction. Further, the evaluation of the SSR for multiple contingencies is performed in [44] by employing a multiway decision tree. Although important developments are presented in the literature to improve the SSR, there is still a need for techniques able to address BPSs with high penetration of RESs.

The initial step in constructing the SSR is clustering the system generators into coherence groups that are operated/dispatched similarly. Traditionally, these groups have been defined based on their geographical location and kept fixed throughout the system operation. However, with the increasing participation of variable RESs, the use of pre-determined generator groups for SSRs may no longer be a viable approach.

1.4.3 BPS Voltage Stability

Voltage stability has been continuously under investigation within the power system industry and academic community given the magnitude of its consequences and direct association to major blackout events worldwide [3]. Several research works have been dedicated to the assessment of BPS voltage stability, including seminal works as continuation power flow methods associated with P-V curve analysis [45], L-index [46], singular value of the load flow Jacobian [47], tangent vector [31] and voltage collapse proximity indicator (VCPI) [48]. In addition, new indexes are recently proposed considering the novel BPS perspectives. The work developed in [49] presents a new voltage stability index based on power flow divergence and decay of voltage magnitude. The study in [50] proposes a new P-index able to indicate the steady-state distance to voltage collapse, as well as dynamic voltage stability. Next, submodular optimization is explored as a tool to prevent voltage instability in [51], whilst ref. [52] seeks to mitigate the risk of voltage stability taking advantage of the increased observability provided by PMUs.

Based on these works, several methods have been proposed seeking the improvement of BPS' voltage stability margins through the insertion of compensation devices. In [53], a strategy based on the bifurcation method is used to determine the optimal location, control, and appropriate sizes of SVCs and thyristor-controlled series compensation (TCSC) to avoid voltage collapse. The work in [4] uses the system-wide voltage stability perspective provided by the tangent vector to determine the most critical locations for reactive power compensation. Heuristic solutions based on the genetic algorithm are explored by [54] and [55] considering

transmission lines loadability constraint and the L-index as optimization criteria. These works seek to determine the locations and capacities for installing flexible AC transmission systems (FACTS), and superconducting magnetic energy storage (SMES). Multi-objective programming approaches for static and dynamic (short-term) voltage stability improvement are developed in [3],[56]. These approaches employ VCPI for quantifying the system voltage stability seeking the adequate placement of static synchronous compensators (STATCOMs) and multi-stage planning for aged SVC equipment retirement.

More recently, new opportunities due to BPS expansion/modernization have been drawing significant attention and motivated important novel studies proposed in the literature. These works take advantage of the significant penetration of RESs and expansion of high-voltage, direct current (HVDC) systems to improve BPSs voltage stability margin without the requirement of new compensators installation. In [57], the reactive power produced by grid-connected variable-speed wind generators is used to enhance the steady-state voltage stability margin. A new perspective considering both active and reactive power injections of photovoltaic systems is proposed in [58] to provide dynamic voltage support to short-term voltage stability. Additional control actions are developed in [59] to utilize VSC-HVDC for global enhancement of steady-state voltage stability. Although, interesting and with meaningful results, the above-mentioned methods somewhat detract from the original design of these systems and may not be of great appreciation in actual operative reality. Consequently, their applicability is limited, as many operators would prefer to run these units at unity power factor, given that active power production is the one typically rewarded [60].

These possible limitations are avoidable using power system FRs' capacity [6]. These resources can have their operation adapted to better accommodate power system requirements without compromising their core values design. Moreover, differently from the above-mentioned applications that may have their actions limited by the requirements of the actual site at which the equipment is installed. FRs are widespread in the network, allowing for their use at the most effective locations to support various power system operation and planning requirements [61]-[66]. In [61] a new assessment of probabilistic flexibility is used to avoid RES power curtailment. Reference [62] presents the application of different emerging FRs as sources of scheduled energy reserve in the electricity market. Further, a new power system expansion planning approach is proposed in [63] considering the participation of FRs aimed at the reduction of new assets acquisition.

Moreover, FRs are especially important to voltage stability support as modern BPS

move toward large integration of variable RESs, which can lead to significant reductions in the system voltage stability margin and variations in the critical location responsible for driving the system to voltage collapse. In [64], curtailable loads are considered as active market participants in heavily loaded systems seeking to ensure voltage stability. The work developed in [65] proposes the application of DR to support voltage control actions while considering the system voltage stability preservation. Next, the work proposed in [66] expands the perspective presented in [65], featuring optimal voltage regulation with DR participation for both primary and secondary control levels. Still, the current state-of-art falls short in the proposal of a method able to take advantage of these distributed controllable resources to ensure secure voltage stability margins.

1.5   Research Objectives

The ultimate goal of this thesis is focused on developing new solutions and analyses enabled by DERs to improve BPS operation and stability in face of the increasing penetration of RES. In this perspective, motivated by these new opportunities, the specific research objectives are described in the following outlined topics, as depicted in the flowchart in Figure 1.2.

First, a novel energy function-based network partitioning is developed for SSR improvement, considering high RESs penetration. This project seeks to take advantage of high precision measurements provided by WAMS associated with PMU to obtain significant enhancement in the observability of modern BPS. Based on this information, a new adaptive definition of the generator-groups is developed significantly improving SSR definition while additional infrastructure is not required.

Second, a novel adaptative area-based voltage stability index is developed. This project takes advantage of new possibilities enabled by DERs, such as FRs, to obtain a meaningful improvement of voltage stability margin and reliability of BPS, while overcoming the early saturation in face of traditional centralized strategies. For this, network-wide sensitivity and the local characteristics of voltage collapse are explored.
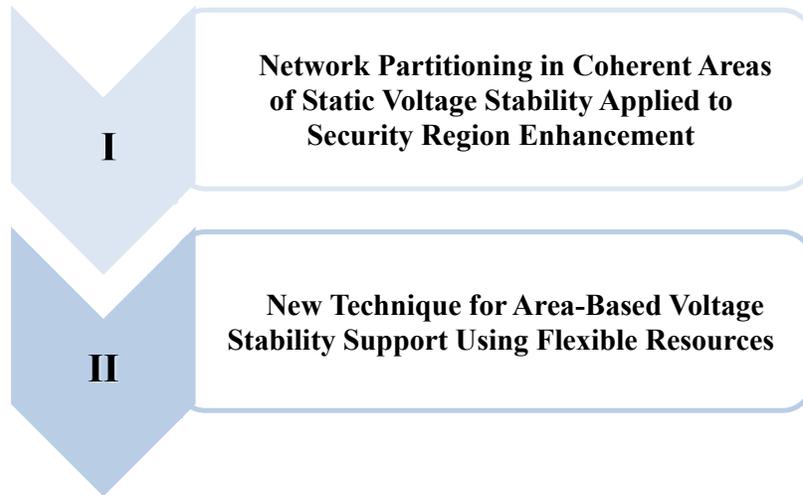
Figure 1.2: Flowchart of research objectives

The flowchart contains:

I — Network Partitioning in Coherent Areas of Static Voltage Stability Applied to Security Region Enhancement

II — New Technique for Area-Based Voltage Stability Support Using Flexible Resources

1.6 Thesis Layout

The remainder of this thesis is structured as follows:

Chapter 1 presents the motivation, background information, literature review, and research objectives to develop the thesis.

Chapter 2 presents preliminaries addressing additional background on major topics required to develop the research objectives.

Chapter 3 presents a novel method for the improvement of the SSR based on a proposed network partitioning algorithm.

Chapter 4 presents a novel area-based outlook using FRs and a new adaptative area-based voltage stability index.

Chapter 6 presents the thesis summary, contributions, and directions for future work.

Chapter 2:   Preliminaries

2.1 Context

This chapter presents the network model representation of BPS and preliminary formulation for energy function applied to BPS, SSR and voltage stability margin.

2.2 Network Model Representation

Consider a BPS with buses contained in the set $\mathcal{N} = \mathcal{N}_{\langle G \rangle} \cup \mathcal{N}_{\langle L \rangle}$, where $\mathcal{N}_{\langle G \rangle}$ and $\mathcal{N}_{\langle L \rangle}$ respectively denote the sets of buses with generation and loads, being possible that a bus is contained in both sets, respectively $\mathcal{N}_{\langle G \rangle} \cap \mathcal{N}_{\langle L \rangle} \neq \emptyset$. The connection between buses is represented by two terminals i and j, where the set of transmission lines is denoted by $\mathcal{V} := \{i, j\} \subseteq \mathcal{N} \times \mathcal{N}$. Let each bus contained in $\mathcal{N}$ be classified under one of the three operative modes: PV, PQ or Vθ, respectively composed in subsets $\mathcal{N}_{\langle PV \rangle}$, $\mathcal{N}_{\langle PQ \rangle}$ and $\mathcal{N}_{\langle V\theta \rangle}$.

2.3 Energy Function Applied to BPS

For static voltage stability, the system energy function is based on the difference between the potential energy of the stable and unstable equilibrium solutions, which are denoted by $X^{(\cdot)} = \{V_i \angle \theta_i\} \mid i \in \mathcal{N}$, respectively $X^s \in \mathbb{X}^s \mid \mathbb{X}^s \subseteq \mathbb{R}^n$ and $X^u \in \mathbb{X}^u \mid \mathbb{X}^u \subseteq \mathbb{R}^{|\mathcal{N}_{PV}| + 2 \cdot |\mathcal{N}_{PQ}|}$, for a respective BPS operating condition $\{P_{\langle spec \rangle}, Q_{\langle spec \rangle}\}$ [85]-[87], where $P_{\langle spec \rangle}$ and $Q_{\langle spec \rangle}$ are the specified active and reactive powers and $|\cdot|$ is an operator that returns the cardinality of a generic set. The stable solution, X^s, consists of the traditional Newton-Raphson load flow operative solution, while the unstable, solution X^u is obtained employing the modified Newton-Raphson load flow method, considering the step-controlled when updating the state variables and a single low voltage solution (LVS) bus, i.e., type-1 solution [88].

The respective bus that should have the LVS associated is defined as the most critical PQ-bus for voltage collapse, $\mathcal{B}^{LVS} \leftarrow \mathcal{B}^C$. This information is accessible early by the highest

absolute value of the tangent vector [31], i.e., for an operating point p preceding a saddle-node bifurcation. As the system approaches voltage collapse, the number of unstable solutions decreases due to the different types of bifurcations that occur before reaching the final saddle-node bifurcation, where X^s and X^u merge, and no further solution exists. In this perspective, at the vicinity of the saddle-node bifurcation, there is only one set of X^s and X^u, enabling the identification of the LVS-bus for a type-1 X^u.

$$\Upsilon(x^s, \lambda) = \left.\frac{dx^s}{d\lambda}\right|_p = -\left[D_{x^s}f|_p\right]^{-1}\left.\frac{\partial f}{\partial \lambda}\right|_p \tag{2.1a}$$

$$\mathcal{B}^C = \left\{(\gamma) : \Upsilon(\gamma) = max\left[abs\left(\Upsilon(x^s, \lambda)\right)\right] \middle| \gamma \in \mathcal{N}_{\langle PQ \rangle}\right\} \tag{2.1b}$$

where $x^s \in \mathbb{R}^{|\mathcal{N}_{\langle PV \rangle}| + 2 \cdot |\mathcal{N}_{\langle PQ \rangle}|}$ denotes the state variables, $\lambda \in \mathbb{R}$ is a scalar parameter that leads the system to the bifurcation manifold $f(x^s, \lambda) = 0$, $f = \mathbb{R}^{|\mathcal{N}_{\langle PV \rangle}| + 2 \cdot |\mathcal{N}_{\langle PQ \rangle}|} \times \mathbb{R} \rightarrow \mathbb{R}^{|\mathcal{N}_{\langle PV \rangle}| + 2 \cdot |\mathcal{N}_{\langle PQ \rangle}|}$ is the non-linear function representing the studied system model, $D_{x^s}f \in \mathbb{R}^{(|\mathcal{N}_{\langle PV \rangle}| + 2 \cdot |\mathcal{N}_{\langle PQ \rangle}|) \times (|\mathcal{N}_{\langle PV \rangle}| + 2 \cdot |\mathcal{N}_{\langle PQ \rangle}|)}$ is the Jacobian matrix and $\frac{\partial f}{\partial \lambda}$ is initially injected by active and reactive power.

With the knowledge of the X^s and X^u, the energy function-based criticality index is calculated. This index is obtained considering a single set of X^s and X^u, which significantly speeds up the energy function parcel calculation, in contrast to the traditional potential energy function that requires an LVS for each bus [86]. This index can be determined for each system bus-i [88] allowing for the quantification of its influence in the system robustness. The lower the value of this index, the greater the influence of the respective bus on the system criticality, otherwise it is described as robust [89].

$$E_{p_i}^u(X^s, X^u) = [V_i^s \cdot I_i^s \cdot \sin(\theta_i^s - \delta_i^s)] \cdot \ln(V_i^u) + [V_i^s \cdot I_i^s \cdot \cos(\theta_i^s - \delta_i^s)] \cdot \theta_i^u +$$
$$\frac{1}{2} \cdot \sum_{\substack{j=1 \\ j \neq i}}^{|\mathcal{N}|} V_i^u \cdot V_j^u \cdot B_{ij} \cdot \cos(\theta_i^u - \theta_j^u) - \sum_{\substack{j=1 \\ j \neq i}}^{|\mathcal{N}|} V_i^s \cdot V_j^s \cdot G_{ij} \cdot \cos(\theta_i^s - \theta_j^s) \cdot \theta_i^u$$
$$- \sum_{\substack{j=1 \\ j \neq i}}^{|\mathcal{N}|} V_j^s \cdot G_{ij} \cdot \sin(\theta_i^s - \theta_j^s) \cdot V_i^u \tag{2.2}$$

where the criticality index of each bus is denoted by $E_{p_i}^u \in \mathbb{R}^{|\mathcal{N}|}$, the vector collecting all buses criticality indexes is represented by $\boldsymbol{E_P^u} = \left[E_{p_1}^u, \dots, E_{p_{|\mathcal{N}|}}^u \right]$, $V_i^s \angle \theta_i^s$ and $I_i^s \angle \delta_i^s$ are the voltage and current phasors measurements, B_{ij} and G_{ij} are transmission lines conductance and susceptance.

2.4 Static Security Region

To assess the BIPS security, the Brazilian Independent System Operator (ONS) employs the software Organon. This tool allows the definition of up to three generator-groups, respectively $\mathcal{G}_1$, $\mathcal{G}_2$ and $\mathcal{G}_3$ [90]-[92]. These generator groups correspond to system interconnected areas, which may be exporting or importing regions employed in the continuation load flow method to control the changes in the system generation pattern.

For this, to visualize the security operation area of the system, three projections ($\mathcal{G}_1 \times \mathcal{G}_2$, $\mathcal{G}_1 \times \mathcal{G}_3$, $\mathcal{G}_2 \times \mathcal{G}_3$) on two-generation subspaces are employed, where $\mathcal{G}_1$, $\mathcal{G}_2$ and $\mathcal{G}_3$ are adaptively modified based on the partitioned coherence areas. In Figure 2.1, the pair-wise analysis of $\mathcal{G}_1$ and $\mathcal{G}_2$ to define the SSR projection $\mathcal{G}_1 \times \mathcal{G}_2$ is depicted. The SSR is calculated from an initial operating point, $\wp_0$, by moving radially in different directions on the plane $\mathcal{G}_1 \times \mathcal{G}_2$, where active power generation of $\mathcal{G}_1$ and $\mathcal{G}_2$ increase or decrease, until it reaches security or a generation limit point. The excess or lack of active power generation resulting from the dispatch of $\mathcal{G}_1$ and $\mathcal{G}_2$ is absorbed by $\mathcal{G}_3$, being the load kept constant during the process.

The number of directions is defined before the beginning of the process and implies a higher resolution of the boundaries. The MW distance between the direction under analysis and the initial operating point is respectively denoted by:

$$\mathcal{D} = \sqrt{\left(P_{\langle \mathcal{G}_1 \rangle} - P_{\langle \wp_{0\mathcal{G}_1} \rangle} \right)^2 + \left(P_{\langle \mathcal{G}_2 \rangle} - P_{\langle \wp_{0\mathcal{G}_2} \rangle} \right)^2 + \left(P_{\langle \mathcal{G}_3 \rangle} - P_{\langle \wp_{0\mathcal{G}_3} \rangle} \right)^2},$$

$$\left(P_{\langle \mathcal{G}_r \rangle}, P_{\langle \wp_{0\mathcal{G}_r} \rangle} \right), \forall\, r \in \mathbb{N}[1,3] \tag{2.3}$$
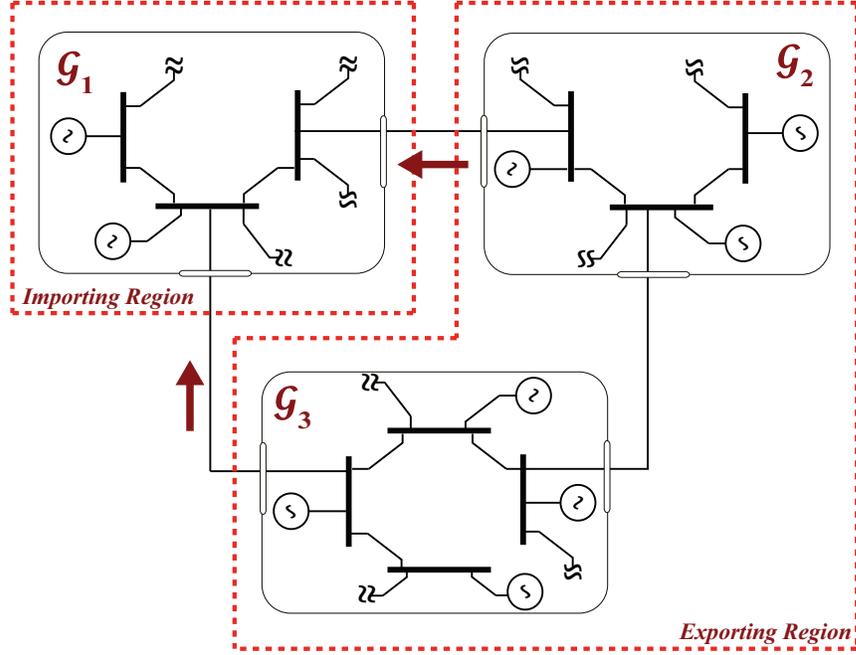
Figure 2.1: Generator-groups definition

SSR, Ω_{SSR}, is composed by the set of operating conditions Ω_{SSR} satisfying the power flow equations, $f(x^s) = P \mid \underline{Q_{\langle G \rangle}} \leq Q_i \leq \overline{Q_{\langle G \rangle}}, \forall\, i \in \mathcal{N}_{\langle PV \rangle}$, and subject to restrictions set $\mathcal{R} = (\mathcal{R}_v \times \mathcal{R}_\theta) \cap \mathcal{R}_G$. For this, $\underline{Q_{\langle G \rangle}}$ and $\overline{Q_{\langle G \rangle}}$ are lower and upper reactive power limits, $\mathcal{R}_V$ is the set of voltage magnitude limits, $\mathcal{R}_\theta$ is the set of thermal transmission limits and $\mathcal{R}_G$ is the set of active power generation limits. Additional limits can be included in the restrictions set $\mathcal{R}$ at the discretion of the system operator, due to the requirements of each analyzed system.

$$\Omega_{SSR} = \left\{ P \in \mathbb{R}^{|\mathcal{N}|} \middle| f(x^s)=P, \forall\, x^s \in \mathbb{R}^{|\mathcal{N}_{\langle PV \rangle}|+2 \cdot |\mathcal{N}_{\langle PQ \rangle}|}, \underline{Q_{\langle G \rangle}} \leq Q_i \leq \overline{Q_{\langle G \rangle}}, \forall\, i \in \mathcal{N}_{\langle PV \rangle} \right\} \tag{2.4}$$

s.t:

$$\mathcal{R}_V = \{ V \in \mathbb{R}^{|\mathcal{N}|} \mid \underline{V_i} < V_i < \overline{V_i}, i \in \mathcal{N} \} \tag{2.5}$$

$$\mathcal{R}_\theta = \{ \theta \in \mathbb{R}^{|\mathcal{V}|} \mid -\overline{\theta_{ij}} \leq \theta_{ij} \leq \overline{\theta_{ij}}, \{i,j\} \in |\mathcal{V}| \} \tag{2.6}$$

$$\mathcal{R}_G = \left\{ P(V,\theta) \in \mathbb{R}^{|\mathcal{N}_{\langle PV \rangle}|} \middle| \underline{P_{\langle G \rangle}} \leq P_i(V,\theta) \leq \overline{P_{\langle G \rangle}}, i \in \mathcal{N}_{\langle PV \rangle} \right\} \tag{2.7}$$

2.5 Voltage Stability Margin

The power system network can be represented by a generic nonlinear model:

$$\mathbf{0} = f(\mathbf{x}, \lambda) \tag{2.8}$$

where $f : \mathbb{R}^{|\mathcal{N}_{\langle PV \rangle}| + 2 \cdot |\mathcal{N}_{\langle PQ \rangle}|} \times \mathbb{R} \to \mathbb{R}^{|\mathcal{N}_{\langle PV \rangle}| + 2 \cdot |\mathcal{N}_{\langle PQ \rangle}|}$ is a nonlinear function with space dimension, $\mathbf{x} = \left[\theta_i, \ldots, \theta_{|\mathcal{N}_{\langle PV \rangle}| + |\mathcal{N}_{\langle PQ \rangle}|}, V_i, \ldots, V_{|\mathcal{N}_{\langle PQ \rangle}|} \right]^T \in \mathbb{R}^{|\mathcal{N}_{\langle PV \rangle}| + 2 \cdot |\mathcal{N}_{\langle PQ \rangle}|} \Big| i \in \mathcal{N}$ denotes the system state variables, $i \in \mathbb{R}$ represents a generic transmission bus, $\lambda \in \mathbb{R}$ is a particular parameter that moves the system from one equilibrium point p to another $p_{[\tau]}$, where $\tau \in \mathbb{R}$ represents the continuation method iteration, and $\mathbf{0} \in \mathbb{R}^{|\mathcal{N}_{\langle PV \rangle}| + 2 \cdot |\mathcal{N}_{\langle PQ \rangle}|}$ represents a vector of all zeros.

The system voltage stability can be studied by driving a known initially stable operating condition up to instability. This instability condition is defined as a bifurcation point and can be divided into two main category groups. The first group represents instability conditions due to the merging of two equilibrium points leading to a null eigenvalue, i.e., characterizing either a saddle-node (SNB), transcritical (TB), or pitchfork bifurcation (PB); or by the crossing of the imaginary axis by a pair of complex conjugate eigenvalues, representing a Hopf bifurcation (HP) [93]. The second group is related to power system operative limits, especially generators reactive power limits, being defined as limited induced bifurcations (LIB). This type of bifurcation occurs due to violations in generators limits, leading to changes in these units operating mode from constant active power and voltage mode, i.e., PV mode, to constant active and reactive power mode, i.e., PQ mode, [94]. This action leads to a new set of equations representing the respective power system that may no longer be stable to the current operating condition, i.e., it may lead to the merging of two equilibrium points with an abrupt crossing of eigenvalues from the right-half plane to the left-half plane side. It should be noted that the literature has consistently demonstrated that voltage collapse is mainly connected to SNBs and LIBs [93],[95].

In this perspective, a widely used approach in the literature to determine the power system's voltage stability margin, i.e., the distance between the current operating point to the point of voltage collapse, or SNB/LIB point, is based on the continuation method. This method is divided into two steps: predictor and corrector. The first step is responsible for increasing the

network load and generation based on a direction of load increase $\lambda_{[\tau]} \in \mathbb{R}$. This direction is assumed to be a known quantity, which is a reasonable assumption provided adequate load forecast [95],[96]. In case that a reliable load forecast is not available, a worst-case direction can be used to ensure that the system presents a satisfactory distance to voltage collapse [97]. Procedures to determine the worst-case direction are detailed depicted in [45],[98].

$$P_{\langle L \rangle_{i,[\tau]}} + j \cdot Q_{\langle L \rangle_{i,[\tau]}} = \left(P_{\langle L \rangle_i} \Big|_{\wp_0} + j \cdot Q_{\langle L \rangle_i} \Big|_{\wp_0} \right) \cdot \lambda_{[\tau]}, \mathbb{C}^{|\mathcal{N}_{\langle PV \rangle}| + |\mathcal{N}_{\langle PQ \rangle}|} \times \mathbb{R} \to \mathbb{C}^{|\mathcal{N}_{\langle PV \rangle}| + |\mathcal{N}_{\langle PQ \rangle}|} \quad (2.9a)$$

$$P_{\langle G \rangle_{i,[\tau]}} = P_{\langle G \rangle_i} \Big|_{\wp_0} \cdot \lambda_{[\tau]}, \mathbb{R}^{|\mathcal{N}_{\langle PV \rangle}|} \times \mathbb{R} \to \mathbb{R}^{|\mathcal{N}_{\langle PV \rangle}|} \quad (2.9b)$$

where $P_{\langle L \rangle_i}$, $Q_{\langle L \rangle_i}$ and $P_{\langle G \rangle_i}$ denote the active and reactive power demands, and active power generation in a generic transmission bus $i \in \mathbb{R}$.

The second step may be performed by solving the power flow problem considering the predictor step as the initial guess. An efficient method to speed up this problem solution is achieved by modeling $\lambda_{[\tau]}$ as an adaptive parameter based on the tangent vector sensitivity [31] and determined by (2.1a).

$$\lambda_{[\tau+1]} = \lambda_{[\tau]} + \rho \cdot \left\| \Upsilon_{[\tau]} \right\|^{-1} \quad (2.10)$$

where $\Upsilon_{[\tau]}$ denotes the tangent vector sensitivity calculated in an equilibrium condition at a generic iteration τ, $\wp \to \wp_{[\tau]}$, and $\rho \in \mathbb{R}$ is a scalar gain used to control the direction increase.

To reduce the expensive computational effort as the system approaches voltage collapse, stopping criteria can be included to terminate the continuation process. The stopping criteria denoted by ξ is a voltage collapse index that can anticipate the vanishing eigenvalue, tending to zero as the bifurcation is approached. It is directly determined from (2.11) for a given operating point having a negligible calculation cost [99]. Ref. [99] also addresses that employing the CRIC method can reduce the computational burden, turning the continuation method eligible for load margins calculation.

$$\xi = \left\| \Upsilon_{[\tau]} \right\|^T \cdot D_x f \Big|_{\wp_{[\tau]}} \cdot \left\| \Upsilon_{[\tau]} \right\| \quad (2.11)$$

Chapter 3: Network Partitioning in Coherent Areas of Static Voltage Stability Applied to Security Region Enhancement

3.1 Context and Overview

In Chapter 1, the literature survey has revealed that there is still a gap in network partitioning methods that take advantage of new technologies such as awareness by WAMS using PMUs. In addition, adaptative SSRs are needed for BPS towards increasing RES penetration. In this perspective, this chapter seeks to address the abovementioned issues. For this, a perspective for SSRs improvement is proposed by adopting a new energy function-based network partitioning method derived from high precision measurements provided by WAMS associated with phasor measurement units PMU. This partitioning method provides an adaptive definition of the generator groups used in SSR construction particularly suited for systems with large penetration of RESs. This allows for the mitigation of RESs intermittency effects, significantly improving the system SSR. Moreover, the use of the energy function for the network partitioning meaningfully enhances the partitioning algorithm robustness, especially in comparison with previously proposed heuristic partitioning approaches [34].

In addition, the use of WAMS provides a precise perspective of the system operating conditions. In this regard, WAMS utilizing PMUs offer a significant enhancement in the observability of power systems compared to traditional supervisory control and data acquisition (SCADA) systems [104]-[106]. The application of WAMS data has been explored in several studies in the literature including secondary voltage control [107], protection techniques [108]-[109], online estimation of transmission lines parameters [110], system restoration [111], short-term frequency prediction [112], reliability and security evaluation [113]. In this chapter, the use of WAMS considering PMU data leads to a superior precision in the calculation of the system energy in comparison with the data provided by traditional state estimation approaches. It eliminates a significant issue in the energy determination regarding the quality of the information obtained through state estimation. This data is highly dependent on the accuracy of the modeled system which can be relatively poor, especially due to the aggregated loads model. Loads are highly dependent on seasonal aspects and can continuously vary their characteristics even during the same operational day period. Furthermore, the load profile is different for

special days with anomalous loads, such as public holidays and long weekends that may vary for each year according to the day of week and seasons [114]. For validation, the system IEEE 118-bus is employed considering different operative scenarios towards the large penetration of variable RESs. Results indicate that the proposed adaptive SSRs can significantly improve the system operational boundaries and enhance its stability margin even when severe variations in the RESs contribution take place. The main contribution of this chapter is its ability to capitalize on the proposed network partitioning based on the potential energy function and WAMS using PMU data, to improve the SSR of power systems with high penetration of renewable resources. The remainder of this chapter is organized as follows: Section 3.2 presents the formulation of the proposed network partitioning based on the energy function index using WAMS and the proposed approach for SSR adaptive formation. In Section 3.3, the proposed methodology is validated presenting obtained results and comparative analysis. Section 3.4 concludes this chapter by summarizing its main findings.

3.2 Proposed Network Partitioning Based on Energy Function Index Using WAMS

In this section, the proposed networked partitioning based on energy function and WAMS is presented.

3.2.1 Energy Function Index with the Aid of WAMS using PMUs

The energy function index considering WAMS associated with PMUs is developed based on the potential energy function formulation depicted in (2.2). Traditionally X^s would be obtained considering state measurements from SCADA systems associated with additional state estimation and load flow calculations. This perspective changes with the recent advancements in transmission system situation awareness provided by WAMS using PMUs. This modern monitoring system allows for more accurate and comprehensive measurement of the system states including wide-area monitoring and the phasor information, i.e., magnitude and angle measurements, which was not previously possible with typical SCADA systems [104]-[106]. Then, this new outlook allows for X^s to be automatically determined from WAMS measurements, avoiding the requirement for supplementary state estimation, since operating

conditions change with RESs intermittency and load variations. These aspects are especially highlighted in this chapter, where the system loading, and consequently its error, is continually increased during the SSR construction until a technical limit boundary is reached.

The determination of LVS at the saddle-node bifurcation point, i.e., voltage collapse point, is a difficult task, and not all LVS may be determined. As changes in the system operating conditions, such as RESs intermittency and load variation can lead to different merged solutions pairs (X^s, X^u) or divergence of the load flow [85]. However, the highly accurate measurements by WAMS using PMU can also aid the definition of X^u once it can provide the precise system operating condition. Then, this allows for the improvement of the X^u determination, as loads aggregated model can be replaced by highly an accurate measurement of the system states, where the voltage phasors $V_i \angle \theta_i$ can aid in the convergence process. In addition, these measurement data provide the initial condition for N-1 buses of the system, as the solution of type-1 is associated with a single bus with a low voltage profile.

3.2.2 Proposed Network Partitioning Method Based on Energy Function

Based on this criticality index the proposed partitioning method is developed. First, the influence of each bus is extended to a system-wide representation in the Cartesian space $r\langle x, y \rangle = x \cdot \hat{\imath} + y \cdot \hat{\jmath}$, denoted by E_{p_i}. Following, the criticality influence of each bus is collected in the system criticality mapping $\Theta(x, y, E_{p_i})$. This process is depicted in (3.1a)- (3.1b).

$$E_{p_i}(x, y, E_{p_i}^u) = E_{p_i}^u \cdot \mathcal{D}_{x_i}(x) \cdot \mathcal{D}_{y_i}(y) \mid i \in \mathcal{N}, E_{p_i}^u \in E_P^u \tag{3.1a}$$

$$\Theta(x, y, E_{p_i}) = \sum_{i \in \mathcal{N}} E_{p_i}(x, y, E_{p_i}^u) \tag{3.1b}$$

where $\mathcal{D}_{x_i} \sim N(d_{x_i}, \sigma^2) \in \mathbb{R}[\underline{x}, \overline{x}] \mid 0 \le \underline{x} < \overline{x} \le \infty$, $\mathcal{D}_{y_i} \sim N(d_{y_i}, \sigma^2) \in \mathbb{R}[\underline{y}, \overline{y}] \mid 0 \le \underline{y} < \overline{y} \le \infty$, N denotes a truncated normal distribution, $x \in \mathbb{R}[\underline{x}, \overline{x}]$ and $y \in \mathbb{R}[\underline{y}, \overline{y}]$ are the system coordinates on the plane $r\langle x, y \rangle$, $d_x = [d_{x_i}, \dots, d_{x_{|\mathcal{N}|}}] \mid d_x \in \mathbb{R}[\underline{x}, \overline{x}]$ and $d_y = [d_{y_i}, \dots, d_{y_{|\mathcal{N}|}}] \mid d_y \in \mathbb{R}[\underline{y}, \overline{y}]$ are buses coordinates.

The parameter $\sigma \in \mathbb{R}_{\geq 0}$ allows to regulate the network partitioning zones, i.e., small σ values lead to a damping of the bus influence, thus providing a large amount of small-sized grid partitioned areas while high σ values lead to a reduced set of areas with many buses.

Based on the mapping Θ, it is desired to define coherence areas, i.e., parcels of the network that have similar behavior. For this, unlike the traditional approaches that achieve areas partitioning based on the construction of a cluster of buses with similar sensitivity [31], the proposed method seeks to perform the network partitioning by directly identifying the boundaries of the coherence areas. These boundaries are extracted from the mapping Θ by identifying transition zones between uncorrelated coherence areas, where a coherence area is defined in the mapping Θ by elevations and valleys containing buses with strong similarity. For this sake, a two steps process is performed.

First, the vector field of the mapping Θ is calculated by its gradient as depicted in (3.2a), where the vector points to the greatest increase of this function. Based on the vector field, it is possible to identify transition regions between coherence areas by monitoring the angle variations of the gradient vectors δ given by (3.2b). This process allows the determination of flow lines passing through zones of change in the vector field direction. The conditions for a transition zone in the vector field are presented in Table 3.1, and an exemplification of its definition is highlighted in the Results section by Figure 3.3(a)-(c), which respectively illustrate the network partitioned areas and the system criticality vector field. In this sense, to identify the system partitioned mapping, a partitioning function Λ is developed, where specifically for (3.2c), the Iverson bracket notation is used. This function assumes the value '1' if the proposition is satisfied, and '0' otherwise, where sgn denotes the signal function. For this, the following propositions are used to identify transition zones:

- The first proposition, denoted by the first and second parcels of (3.2c), seeks to identify slow transitions within coherence areas. This is achieved using a slack variable ξ which represents the angular deviation that a gradient vector can be within for the identification of a transition zone.

- The second proposition, denoted by the third and fourth parcels of (3.2c), addresses strong transition zones. These conditions address cases where neighbor gradients change direction abruptly without going through the transition criteria depicted in Table 3.1. In these cases, the perception of a boundary is possible by identifying signal changes of the vector field in either direction. The partitioned map of the system, $r_{\mathcal{A}}$, is obtained by evaluating the mapping of $\mathcal{F}$ for a plane $\hat{\imath}, \hat{\jmath}$ at $\Lambda = 1$. The complete process is depicted in (3.2a)-(3.2d).

Table 3.1: Transition region conditions

$(\vec{\nabla}\Theta)$	$\tan\delta = \left\|\dfrac{\mathcal{D}y}{\mathcal{D}x}\right\|$	δ
$r\langle\pm1,0\rangle$	0	0
$r\langle0,\pm1\rangle$	∞	$\pi/2$

$$\vec{\nabla}\left(\Theta(x,y,E_{p_i})\right) = \frac{\partial\left(\Theta(x,y,E_{p_i})\right)}{\partial x}\hat{\imath} + \frac{\partial\left(\Theta(x,y,E_{p_i})\right)}{\partial y}\hat{\jmath} \tag{3.2a}$$

$$\delta(x,y) = \tan^{-1}\left|\frac{\mathcal{D}y(x,y)}{\mathcal{D}x(x,y)}\right| \tag{3.2b}$$

$$\Lambda(x,y) = \left[\left([\delta(x,y) - \xi \leq 0] + \left[\delta(x,y) + \xi \geq \frac{\pi}{2}\right]\right.\right.$$
$$\left.\left.+ \frac{1}{2}\left|\frac{\partial\{\text{sgn}(\mathcal{D}x(x,y))\}}{\partial x}\right| + \frac{1}{2}\left|\frac{\partial\{\text{sgn}(\mathcal{D}y(x,y))\}}{\partial y}\right|\right) > 0\right] \tag{3.2c}$$

$$\boldsymbol{r}_{\mathcal{A}} \leftarrow \mathcal{F}\left(\mathbb{X},\mathbb{Y},\Lambda(x,y)\right) \mid \Lambda(x,y) = 1, \quad \mathbb{X} = \mathbb{R}[\underline{x},\overline{x}], \mathbb{Y} = \mathbb{R}\left[\underline{y},\overline{y}\right] \tag{3.2d}$$

Next, a second stage is developed allowing one to perform the clustering of small coherence areas into larger coherence areas. This step is necessary as the first stage can lead to an extensive division of the system in several small coherence areas. For this, the divergence of the vector field map denoted by $\nabla\left(\vec{\nabla}(\Theta)\right)$ in (3.3a) is used to provide a scalar measure of the transition zones likeness of defining a boundary for larger coherence areas. A transition zone with a low divergence index implies strong dissimilarity between the neighbors' small coherence areas, therefore it should be preserved, while transition regions with significant divergence levels indicate that the neighbors' small coherence areas can be clustered. To perform the areas clustering a new partitioning function K is developed in (3.3a) using the Iverson brackets notation to establish a comparison proposition between the transition regions divergence levels with a partitioning index $\zeta_A \in \mathbb{R}_{\geq0}$. For this, small values of ζ_A lead to the system partitioning into large coherence areas, while the increasing of ζ_A yields to more sub-divisions up to the system comprehensive partitioned map $\boldsymbol{r}_{\mathcal{A}}$, i.e., $\lim_{\zeta_A\to\infty} K(x,y) = \Lambda(x,y)$.

The clustered partitioned map of the system, $r_{\mathcal{K}}$, is obtained by evaluating the surface $\mathcal{F}$ for a plane $\hat{\imath}, \hat{\jmath}$ at $K = 1$, as described in (3.3b).

$$K(x, y) = \left[\left| \nabla \left(\vec{\nabla} \left(\Theta(x, y, E_{p_i}) \right) \right) \right| \circ \Lambda(x, y) \leq \zeta_A \right] \tag{3.3a}$$

$$r_{\mathcal{K}} \leftarrow \mathcal{F}(\mathbb{X}, \mathbb{Y}, K(x, y)) | K(x, y) = 1 \tag{3.3b}$$

where the operator '$\circ$' denotes the element-wise product.

3.2.3 SSR Considering Adaptive Network Partitioning

Variations in a system operating condition, especially when facing great penetration of intermittent RESs, can significantly affect the network coherence areas. In this perspective, the proposed network partitioning method is employed to adaptively determine the generator groups for SSRs evaluation, which is depicted in the formulation presented in (**2.3**)-(2.7). In this perspective, each group generator is adaptively associated with a proposed coherence area. It should be noticed that the consideration of WAMS using PMU high-resolution measurements allows the proposed method to effectively address variabilities and uncertainties associated with RES, as in practice, a few minutes are tolerated for the system actions, i.e., it is assumed that system states do not change significantly during a tolerance period [117], where the completion of the system SSR assessment should be available before this period ends. In case the SSR construction time needs to be improved, additional computing capacity may be added [117].

A detailed description of the process to obtain the proposed partitioning for SSR is depicted in Figure 3.1.
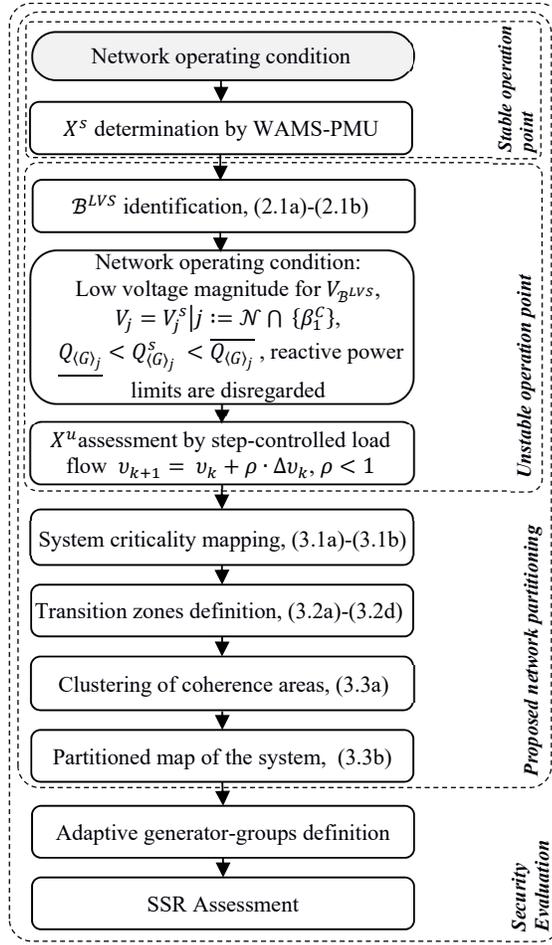
Figure 3.1: Proposed network partitioning method for SSRs improvement

3.3 Results

In this section, the proposed robust network partitioning into coherence areas for the adaptive definition of generator groups for SSRs assessment is verified through case studies simulations. For this, the IEEE 118-bus system [118] is employed considering modifications to represent the BPS movement toward modern monitoring infrastructures by WAMS using PMU and large penetration of variable RESs, which represent 20.0% of generation installed capacity. In this sense, it is considered that each bus has the voltage and current phasors measured by a PMU connected to a centralized WAMS [104]-[105], as defined on BIPS. In BIPS, the monitoring performed by WAMS using PMU has a centralized communication system associated with a central control center located in the South region [115]-[116]. In addition, the available sources are uniformly distributed, considering partitioned areas in Case 0, i.e., 0.6

GW of solar generation and 0.4 GW of hydro generation placed in the second partitioned area, while 1 GW of wind generation is allocated in the third partitioned area. These buses correspond respectively to the loss-sensitive [4] and critical [31] buses of the second and third coherence areas, defined by the partitioning algorithm in Case 0. These respective buses are depicted in Table 3.2. In addition, the generation and voltage limits are depicted in Table A.1 in Appendix A.

Table 3.2: Generation allocation in the IEEE 118-bus system

Generation type	Buses
Solar	51,52,50,58,53,57,67,63,64
Wind	39,33,35,117,43,2,13,14,3,16,37,20,7,11,29
Hydro	118,75,45,47,48,71

Based on these considerations four case studies are developed to represent different operational conditions of modern BPS in face of intermittent RESs penetration. Following, the developed case studies investigation is divided into two main analyses for proposed network partitioning and the new SSR approach. First, a comparative analysis is presented between the proposed network partitioning method and the literature. Next, the novel SSR approach is investigated. This analysis demonstrates the ability of the proposed network partitioning method to improve adaptatively the SSRs definition of modern BPS.

The developed case studies are following described:

- Case 0 denotes the system with traditional settings (base-case) and provides a comparative result for validation of the proposed network partitioning method with traditional approaches available in the literature.

- Cases I-III represent the modern BPSs toward large expansions of its energy matrix by variable RESs. These case studies seek to demonstrate the impact of RESs intermittence in the proposed network partitioning and consequently how this proposed method can significantly improve SSRs. In this sense, three boundary conditions for BPS operation are evaluated. Case I depicts high contributions from solar and wind generations; Case II considers the change in weather conditions, leading the system to low contribution from wind generation, i.e., 10% of its generation capacity, and high level of solar generation; and Case III assumes an opposite scenario of Case II, featuring a low solar generation, i.e. 10% of its generation capacity, and high wind generation.

3.3.1 Network Partitioning Validation

To demonstrate the applicability and effectiveness of the new network partitioning method, this proposed algorithm is implemented in Matlab. For this, first X^s and X^u are obtained for system criticality index evaluation as depicted in Section 2. The respective bus associated with the LVS is determined based on the tangent vector information for each case, being respectively associated to $B^C = 41$. Next, the proposed network partitioning method is performed considering $\{\sigma = 10, \xi = 10°, \zeta_A = 0.34\}$. The obtained system coherence areas for Cases 0, I, II, and III are denoted by $\mathcal{A}_r^{\langle s \rangle} \subseteq r_{\mathcal{K}}, \forall \ r \in \mathbb{N}[1,3]$, $s \in \{I, II, III\}$, where the superscript s represents Cases I-III, while for Case 0 is omitted. The subscript r indicates each system area number, being sorted based on each area criticality towards voltage collapse, i.e., subscript '1' is more critical than '3'.

The obtained partitioned areas by the proposed method in Case 0 are compared with the graphical partitioning algorithm presented in [19]. The results present high similarity between the obtained partitioned areas by both methods, showcasing the effectiveness and suitability of the proposed method. This comparison of the respective network partitioned areas is shown in Figure 3.2, where three areas are identified and the dashed contours denote the partitioned areas depicted in [19], while solid contours denote proposed partitioned areas. In addition, the respective buses which changed the area are summarized in Table 3.3.
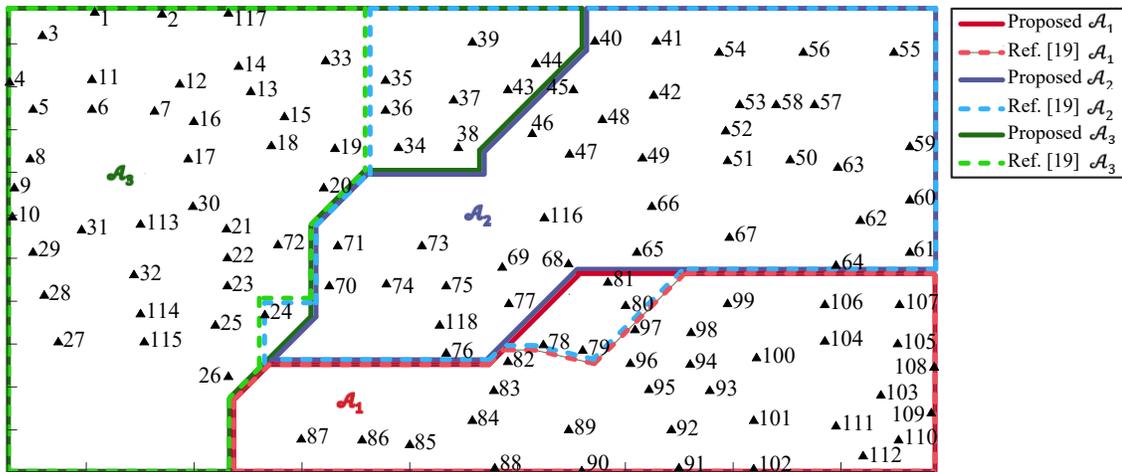

Figure 3.2: Comparison between partitioning of the system IEEE 118-bus modified for the proposed method and ref. [19] in Case 0

Table 3.3: Difference between the proposed and ref. [19] network partition

Proposed Area	$\mathcal{A}_1$	$\mathcal{A}_2$	$\mathcal{A}_3$
Bus	78, 79, 80, 81	24	34, 35, 36, 37, 38, 39, 43, 44

In Figure 3.2, the transmission lines and generators representation are suppressed to improve the visualization of the partitioned areas. Next, the obtained network partitioning for Cases I-III is depicted in Figure 3.3(a)-(c) following the same representation of Figure 3.2, and additionally the respective vector field of each criticality mapping is represented by light green arrows. In Figure 3.3(a) details in the coherence areas boundary are shown to illustrate the respective conditions for the definition of the transition zones between coherence areas. As one can observe zoomed parcel of the vector field highlighted in Figure 3.3(a), there is a change in the direction of gradient vectors in the vector field. This change is detected by the proposed partitioning formulation (3.2c) leading to the identification of the coherence areas boundaries. Then, it is possible to observe that both propositions used to identify transition zones in (3.2c) are satisfied.

First, recalling the proposition depicted in (3.2c) which states that a system region represents an area boundary in case that its gradients angles, $\delta(x,y)$, are within an angular deviation ξ to the transition conditions, i.e. $[\delta(x,y) - \xi \leq 0]$ or $\left[\delta(x,y) + \xi \geq \frac{\pi}{2}\right]$. One can notice, analyzing the zoomed parcel of the vector field highlighted in Figure 3.3(a), that this condition is satisfied, i.e. the respective gradients are pointed downward perpendicularly, leading to a true value for the relation $\delta(x,y) + \xi \geq \frac{\pi}{2}$. The sole fulfillment of this condition would be enough to determine that this parcel of the system represents an area boundary. Still, the second proposition is also fulfilled. For this proposition, the gradient vectors' projections along with directions $\hat{\imath}$ and $\hat{\jmath}$ are used to identify strong transition zones, i.e., changes in the direction of the vector field. The analysis of the projections along the direction $\hat{\imath}$ indicates that the gradient vectors are pointing to opposite directions, this is verified by evaluating the derivate of the projections signal in the respective direction of interest, i.e., $\frac{1}{2}\left|\frac{\partial\{\text{sgn}(\mathcal{D}x(x,y))\}}{\partial x}\right| = 1$.

Further, comparing the obtained network partitioning in Figure 3.3(a)-(c), one can observe that the variation in the renewable's contributions can significantly affect the coherence areas definition. Analyzing Cases I-III, it is noticed that all cases showed different partitioned areas. Cases I and II present similar coherence areas, this occurs once the area where wind generators are allocated, i.e., $\mathcal{A}_3^{(I-II)}$ in Cases I-II, is the area that has the lowest criticality level

to voltage collapse. In this sense, variations in the wind-based RESs intermittency do not significantly impact the system coherence areas division. Moreover, even though the analyzed scenario represents a significant reduction in this area generation contribution, which consequently increases the criticality level of this region, its impact is not meaningful enough to majorly influence the system areas partitioning.

In contrast, the analysis regarding solar-based RES intermittency performed by Case III indicates that a low contribution of solar generation leads to significant changes in the system coherence areas clustering. In this scenario, the criticality index of the area in which these sources are mainly allocated, i.e., $\mathcal{A}_2^{\langle III \rangle}$, is significantly increased. This leads to the expansion of $\mathcal{A}_3^{\langle III \rangle}$, which now presents greater similarity to the sub-region comprising the newly included hydro generators previously associated to $\mathcal{A}_2^{\langle I-II \rangle}$ in Cases I-II. This situation takes place in Case III once the transition zones between the respective sub-region and $\mathcal{A}_2^{\langle III \rangle}$ assumes a low divergence index, which implies strong dissimilarity between them, whereas the transition zones with $\mathcal{A}_3^{\langle III \rangle}$ present a greater divergence index, therefore leading to its clustering. This process is depicted by (3.3b).
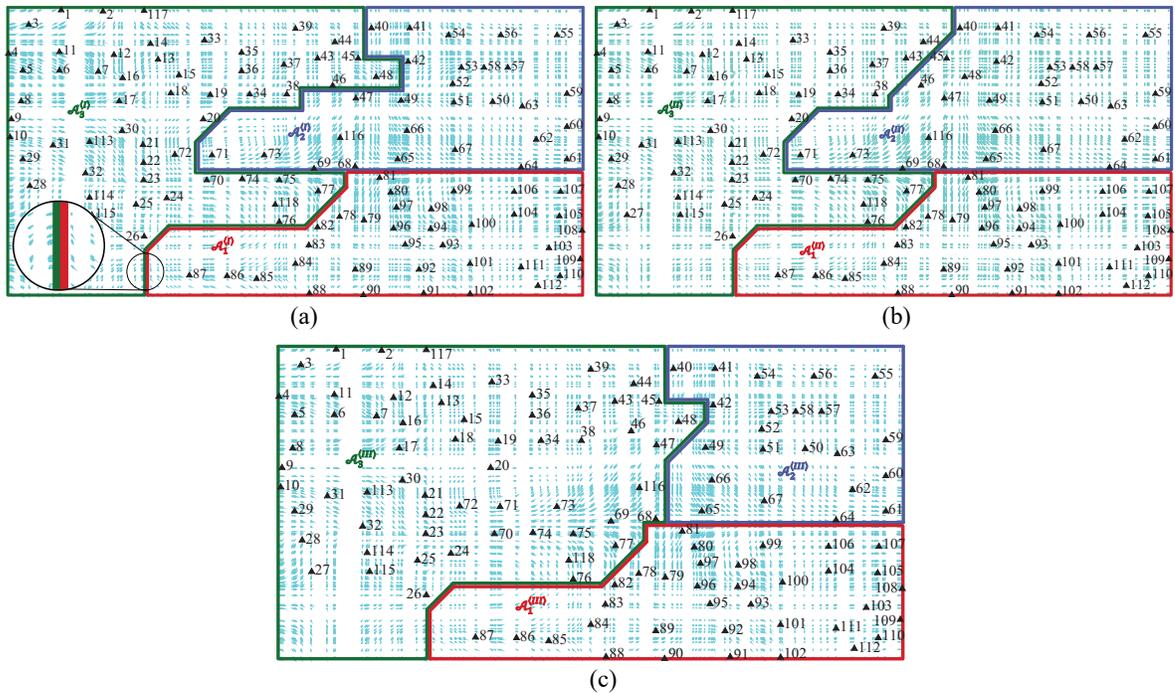

Figure 3.3:Partitioning of the system IEEE 118-bus modified (a) Case I; (b) Case II; (c) Case III

3.3.2 Proposed Adaptive Static Security Region Assessment

Based on the obtained network partitioning by the proposed method for Cases I-III, this section seeks to showcase the capacity of the proposed approach to improve the SSRs, especially in modern BPSs with large RESs contributions. Traditionally, the SSR assessment is performed considering pre-established generator groups that are not adjusted along with the system operation [90],[117]. The SSRs and generator-groups for the traditional approach can be denoted by $\Omega_{SSR}^{\odot,\langle s \rangle} \leftarrow \mathcal{G}_r^s \leftarrow \mathcal{A}_r^{\odot,\langle s \rangle} \big| \mathcal{A}_r^{\odot,\langle s \rangle} = \mathcal{A}_r^I, \forall\, r \in \mathbb{N}[1,3], s \in \{I, II, III\}$, where $\Omega_{SSR}^{\odot,\langle s \rangle}$ denotes the system SSR, $\mathcal{G}_r^s$ consists of the generator-groups contained in the respective system partitioned areas $\mathcal{A}_r^{\odot,\langle s \rangle}$, and the superscript $\odot$ represents the traditional case. In this perspective, seeking to take advantage of the increasing monitoring capacity of modern power systems to improve the boundaries of their operating regions, i.e., SSRs, the proposed approach considers the changes in the system operating conditions to adaptively determine the generator-groups for the SSRs assessment. This is based on the variations in the system partitioned coherence areas. The proposed SSRs and generator groups are denoted by $\Omega_{SSR}^{\otimes,\langle s \rangle} \leftarrow \mathcal{G}_r^s \leftarrow \mathcal{A}_r^{\otimes,\langle s \rangle} \big| \mathcal{A}_r^{\otimes,\langle s \rangle} = \mathcal{A}_r^{\langle s \rangle}, \forall\, r \in \mathbb{N}[1,3], s \in \{I, II, III\}$, where the superscript $\otimes$ represents the proposed approach.

The obtained results for each case study including the three projections ($\mathcal{G}_1 \times \mathcal{G}_2$, $\mathcal{G}_1 \times \mathcal{G}_3$, $\mathcal{G}_2 \times \mathcal{G}_3$) are depicted in Figure 3.4-Figure 3.6, where the solution representing the initial operation condition, i.e. starting point for the SSR construction, is indicated by an 'x' for the proposed method $\mathcal{P}_{0_{\mathcal{G}}}^{\otimes}$, and 'o' for the traditional method $\mathcal{P}_{0_{\mathcal{G}}}^{\odot}$. Analyzing Figure 3.4-Figure 3.6 one can clearly observe that the proposed network partitioning considering WAMS data to determine the generator-groups for SSR assessment, leads to significant improvements in the system SSRs for all studied cases. The SSRs obtained considering the proposed approach have significantly higher operating regions, which allow greater flexibility for the system operation, including more room for control actions and operating maneuvers, maintenance requests, and unforeseen operating scenarios.

Further, the results indicate that several operating conditions that could not be fully secured by the traditional method become operational when the proposed method of the generator-groups adaptive determination is considered. It can be observed in Figure 3.4-Figure 3.6, e.g. for $P_{\langle \mathcal{G}_1 \rangle} = 0.3$ GW, $P_{\langle \mathcal{G}_2 \rangle} = 1.0$ GW and $P_{\langle \mathcal{G}_3 \rangle} = 0.8$ MW, which is defined as a secure scenario in Cases I-III by the proposed approach, however, it is classified as unsafety by the

traditional SSRs in all of them. This result is possible due to the proposed area updating applied to SSR, as it can account for the impact of RESs intermittency in the definition of the system coherence areas, which are later used to adapt the system generator-groups leading to the adaptive SSRs with major improvements as depicted in Figure 3.4-Figure 3.6 for Cases I-III.

Next, seeking to quantify and illustrate the proposed approach improvement capacity, Table 3.4 is developed. It presents a summary of the highest direction variations, i.e., the distance between the initial point and SSR boundary, the type of limit violated, and a ratio of improvement denoted by $\Psi_{\mathcal{D}} = \mathcal{D}^{\otimes}/\mathcal{D}^{\odot}$ quantifying the proposed approach improvement capacity.

From Table 3.4, one can observe the expressive improvements enabled by the proposed approach for the system SSRs for the distinct operating scenarios, where the smallest ratio of improvement $\Psi_{\mathcal{D}}$ obtained in the analyzed case studies, features a 200% ratio of improvement in comparison with the traditional SSR approaches.

Table 3.4: Performance evaluation for each case-study

Case-study	Method	Direction	Limit type	$\mathcal{D}$ (MW)	$\Psi_{\mathcal{D}}$
I	Proposed	11	$\underline{V_{33}}$	947.2	300%
	Traditional	11	$\underline{V_{33}}$	316.1	
II	Proposed	11	$\overline{P_{\mathcal{G}_3}}$	1644.4	279%
	Traditional	11	$\overline{P_{\mathcal{G}_3}}$	589.4	
III	Proposed	1	$\overline{P_{\mathcal{G}_1}}$	1213.5	214%
	Traditional	1	$\underline{V_{33}}$	566.7	

(a)

(b)

(c)
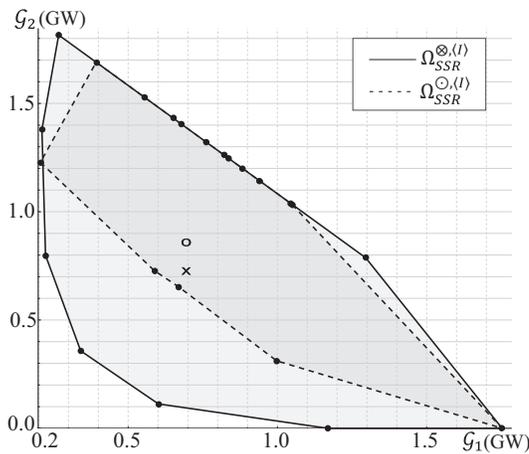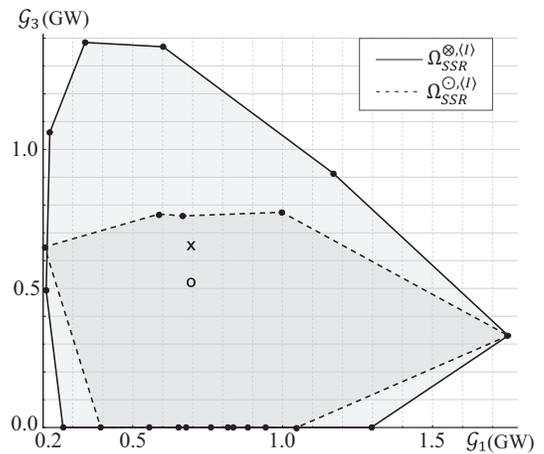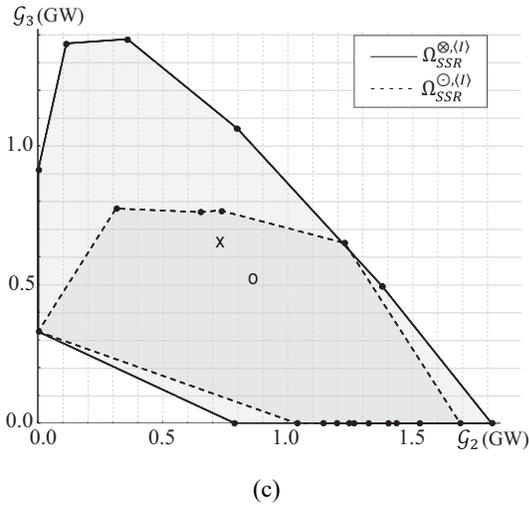
Figure 3.4: SSRs for the IEEE 118-bus system considering high renewable generation in the second and third areas (Case I) (a) $\mathcal{G}_1 \times \mathcal{G}_2$; (b) $\mathcal{G}_1 \times \mathcal{G}_3$; (c) $\mathcal{G}_2 \times \mathcal{G}_3$

(a)

(b)

(c)
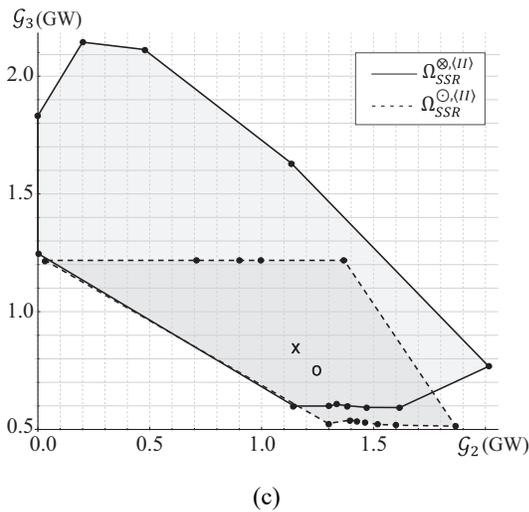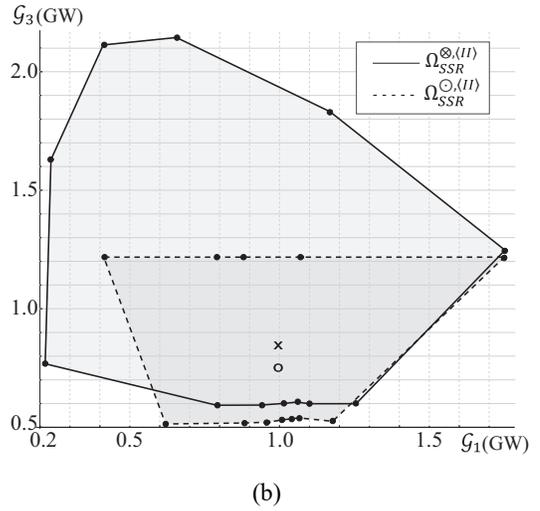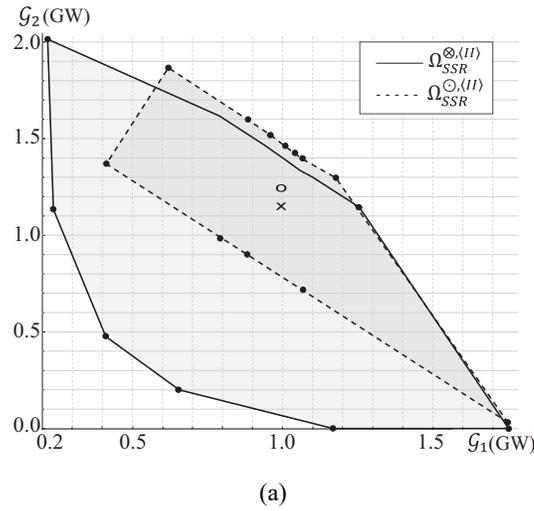
Figure 3.5: SSRs for the IEEE 118-bus system considering high solar generation in the second area (Case II) (a) $\mathcal{G}_1 \times \mathcal{G}_2$; (b) $\mathcal{G}_1 \times \mathcal{G}_3$; (c) $\mathcal{G}_2 \times \mathcal{G}_3$

(a)

(b)

(c)
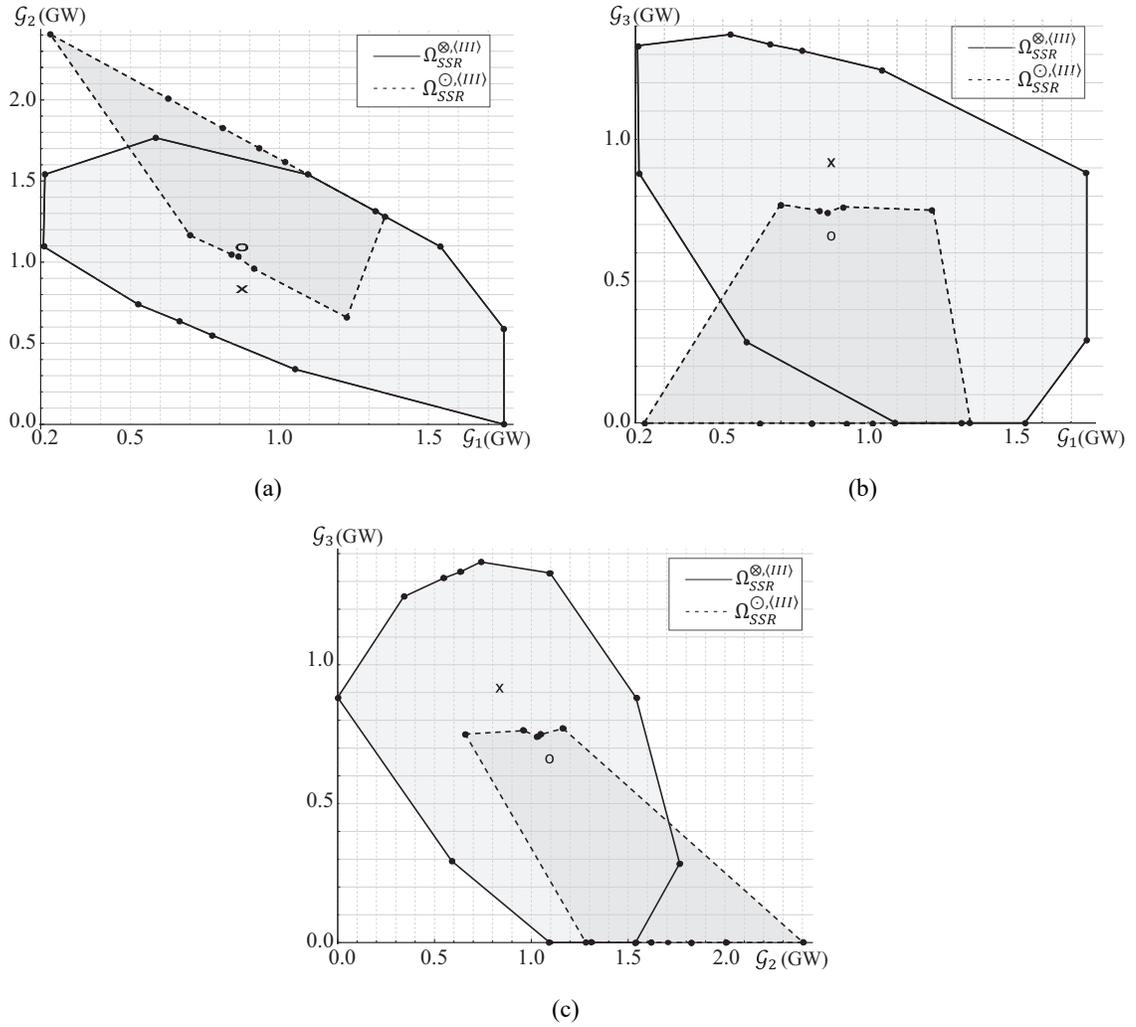
Figure 3.6: SSRs for the IEEE 118-bus system considering high wind generation in the third area (Case III) (a) $\mathcal{G}_1 \times \mathcal{G}_2$; (b) $\mathcal{G}_1 \times \mathcal{G}_3$; (c) $\mathcal{G}_2 \times \mathcal{G}_3$

3.4 Summary

In this chapter, a novel network partitioning is proposed based on the potential energy function and WAMS using PMU data for SSR improvement in the short-term. For this, a comprehensive mapping of the system criticality is developed and used to determine its coherence areas. Next, the partitioned areas are employed to adaptively determine the generator-groups for the system SSR evaluation, therefore, the RESs intermittency influence the system coherence areas boundaries and counter-acting to improve the system security margin. The proposed network partitioning is validated with the literature and the proposed adaptive SSR method is tested considering distinct operating scenarios faced especially by

modern BPSs. The case studies provide a broad perspective of the system SSR behavior and a meaningful validation of the proposed method. Moreover, these case studies demonstrate the significant impact of RESs intermittency in the network partitioning, and the capacity of the proposed method to mitigate this effect and improve the systems SSRs without the requirement of additional infrastructures. The results indicate that the proposed SSR method allows operating conditions previously deemed unsafe by the traditional perspective to become operational as the adaptive definition of the generator-groups is featured. The main contributions of this chapter are following summarized:

- Consideration of WAMS using PMU for precision improvement of the system criticality index determination.
- An energy function-based network partitioning method that determines the system criticality and extracts coherence areas boundaries considering transitions zones.
- Proposal of an adaptive SSR method that considers the system operating conditions to adapt SSR's generator-groups based on the system network partitioning.

Chapter 4:   New Technique for Area-Based Voltage Stability Support Using Flexible Resources

4.1 Context and Overview

In Chapter 1, the literature review has shown that there is still a gap to ensure voltage stability margins for modern BPS. Based on the major opportunities enabled by FRs and the new voltage stability requirements of modern BPS, this chapter proposes a novel area-based voltage stability index. The proposed index seeks to provide a direct measure for FRs' dispatch, to guarantee reliable voltage stability margins for modern BPSs with significant penetration of RES generation. For this, the proposed approach is composed of four main steps, respectively 1) voltage stability margin determination, 2) system-wide sensitivity, 3) local area-based sensitivity, and 4) proposed index derivation. To perform these steps, knowledge of the system's current operating condition, i.e., loading, generation and system parameters, and forecasted direction of load increase is required. Using this information, first the system voltage stability margin is assessed employing the continuation method. Based on this result, a system wide-sensitivity is derived indicating the susceptibility of each bus to lead the system to voltage collapse. From this overall perspective, multiple coherence areas are determined, and local area-based sensitivities are obtained. This information is used in the development of the proposed sensitivity index, providing a direct multi-area perspective for FRs' dispatch.

To validate the proposed approach, comparative simulation case studies are performed in MATLAB considering the IEEE 118-bus test system with modifications to reflect the progress of modern BPSs toward large penetration of RESs and FRs. In this environment, the proposed approach is stressed with several case studies respectively divided into 1) Validation and performance evaluation, 2) Sensitivity analysis 3) Comparative analysis between FRs and RESs operation under voltage control for voltage stability support. These case studies showcase the need for voltage stability support in systems with significant penetration of RESs while depicting the superior ability of the proposed approach to ensure safe operative conditions.

This perspective is depicted in Table 4.1, presenting a comparison between available works in the literature and the proposed approach.

Table 4.1: Comparison with literature state-of-art

	Static VAR compensation	VSC-HVDC	Load curtailment	RES	Flexible resources				Voltage control	Voltage stability	Secure voltage stability margin	RES curtailment reduction	Expansion planning	Schedule energy reserve	Direct system-wide solution method	Direct area-based solution method	Iterative solution method
					DR	ESS	EV	DG									
Ref. [49]										×					×		
Ref. [50]			×							×					×		
Ref. [64]			×							×							×
Ref. [59]	×	×								×					×		×
Ref. [51]	×								×	×					×		×
Ref. [65]	×		×	×	×				×	×							×
Ref. [66]	×		×	×	×				×	×							×
Ref. [61]			×			×		×						×	×		
Ref. [63]			×	×	×			×					×				×
Ref. [62]			×	×	×	×	×	×						×			×
Proposed			×	×	×		×	×		×	×				×	×	

The remainder of this chapter is organized as follows: Section 4.2 and 4.3 respectively present the load model and FRs formulation. Section 4.4 depicts the proposed area-based voltage stability support. Section 4.5 validates the proposed index presenting obtained results and comparative analysis. Section 4.6 concludes this chapter by summarizing its main findings.

4.2 Load Model

Loads composition is denoted by a regular non-controllable portion and an aggregated flexibility parcel, respectively denoted by $k_i \in \mathbb{R}$ and $\varphi_{i,\langle flex \rangle} \in \mathbb{R}$ for a generic bus i.

$$P_i = P_{\langle L \rangle_i} \cdot \left(1 - \varphi_{\langle flex \rangle_i}\right),\ 0 \leq \varphi_{\langle flex \rangle_i} < 1 - k_i \tag{4.1}$$

$$P_{\langle L \rangle_i} = P_{\langle L \rangle_{0_i}} \cdot \left[\alpha_{\langle p \rangle_i} \cdot \left(\left| \frac{V_i}{V_{0_i}} \right| \right)^2 + \beta_{\langle p \rangle_i} \cdot \left(\left| \frac{V_i}{V_{0_i}} \right| \right) + \gamma_{\langle p \rangle_i} \right] \tag{4.2}$$

where $\alpha_{i\langle p \rangle} \in \mathbb{R}$ denotes the constant impedance (Z) share for a generic bus i, constant current (I) and power (P) shares are defined by $\beta_{\langle p \rangle_i} \in \mathbb{R}$ and $\gamma_{\langle p \rangle_i} \in \mathbb{R}$, being the participation

coefficients subjected to the relation $\left\{\left(\alpha_{\langle\cdot\rangle_i} + \beta_{\langle\cdot\rangle_i} + \gamma_{\langle\cdot\rangle_i}\right) = 1 : \left[\alpha_{\langle\cdot\rangle_i}, \beta_{\langle\cdot\rangle_i}, \gamma_{\langle\cdot\rangle_i}\right] \in \mathbb{R}_{\aleph}^3 \mid \mathbb{R}_{\aleph} = [0,1]\right\}, \forall\, i \in \mathcal{N}_{(L)}$, $V_i \in \mathbb{C}$ denotes the nodal phase voltage. The interested reader in the process of FRs' aggregation is referred to [119].

4.3 Flexible Resources

Power system flexibility represents the network capacity to capitalize on the system's available resources to respond to net demand change requests [120]. This perspective is available through different power system elements [121], out of which this work is focused on three main categories namely DR, DG, and EVs.

DR is the ability of the system to manage its load through intentional curtailment, nominal supplied power adjustment, or time-shifting of specific groups of interruptible loads due to operation requirements [65]. This perspective is the following model for a generic bus i by the respective model depicted in [122].

$$P_{\langle DR\rangle_i} = \sum_{a \in A_i} p_i^a, \qquad \mathcal{P}_{A_i} = \left[p_i^1, \dots, p_i^{|A_i|}\right] \tag{4.3}$$

where $P_{\langle DR\rangle_i}$ is the total nodal i DR capacity, A_i is set of interruptible/adjustable loads connected at bus i, p_i^a denotes the corresponding load demand for each load $a \in A_i$.

Following, distributed generation enables the injection of specific controllable contributions of power to the grid. These contributions are limited by their current dispatching power and respective rated generation capacity [123].

$$\left\{ P_{\langle DG\rangle_i} : \ \underline{P_{\langle DG\rangle_i}} \leq P_{\langle DG\rangle_i} \leq \overline{P_{\langle DG\rangle_i}}, \qquad \left(P_{\langle DG\rangle_i}\right)^2 + \left(Q_{\langle DG\rangle_i}\right)^2 \leq \left(\overline{S_{\langle DG\rangle_i}}\right)^2 \right\} \tag{4.4}$$

where $P_{\langle DG\rangle_i}$ and $Q_{\langle DG\rangle_i}$ represent the unit current active and reactive power generation, $\underline{P_{\langle DG\rangle_i}}$ and $\overline{P_{\langle DG\rangle_i}}$, denote minimum and maximum active power generation, and $\overline{S_{\langle DG\rangle_i}}$ denotes the DG-rated power.

In addition, equipment as EVs may perform both above-mentioned flexibility possibilities simultaneously [124]-[125]. These units may have their charging process

interrupted or adjusted representing DR actions. As well as, contributing with power injections in a similar way as a DG due to their ESS capacity. In this sense, these units' flexibility is presented as an association of DR and DG.

$$P_{\langle EV\rangle_i} = \sum_{k \in EV_i} p_i^k + p_{\langle DG\rangle_i}^k,$$

$$\left\{ (p_i^k, p_{\langle DG\rangle_i}^k): \ 0 \le p_i^k \le \tilde{p}_i^k \le \overline{P_{charge_i}^k}, \ \ 0 \le p_{\langle DG\rangle_i}^k \le \overline{P_{discharge_i}^k} \right\}$$

(4.5)

where $\tilde{p}_i^k$ denotes the EV current charging power, p_i^k represents the EV reduction of charging power, i.e., DR, $p_{\langle DG\rangle_i}^k$ is the power injection provided by the respective EV, i.e., DG. $\overline{P_{charge_i}^k}$ and $\overline{P_{discharge_i}^k}$ are the EV charger maximum charging and discharging power.

4.4   Proposed Area-based Voltage Stability Support

Based on the voltage collapse information the proposed area-based sensitivity index is developed. For this sake, a novel methodology composed of three main stages is proposed: 1) system-wide perspective for the definition of most critical buses; 2) area-based sensitivity providing the characterization of critical cores and coherence areas; and 3) area-based voltage stability index responsible to determine the most effective buses and their respective contribution for voltage stability support.

First, a system-wide sensitivity is obtained indicating the susceptibility of each bus to lead the system to voltage collapse. This sensitivity is achieved through the calculation of the tangent vector by (2.1a) at the vicinity of the voltage collapse point denoted by $\Upsilon_\# :=$ $dx/d\lambda|_{\wp \to \wp_\#}$; reference on this voltage stability technique is available in [31]. Based on this information, the PQ-buses criticality indexed by $\Upsilon_\#^{PQ}$ are extracted from the full set $\Upsilon_\#$, and a ranking is performed to identify the most and least effective buses for voltage stability support, respectively denoted by the set $B^\dagger = \{\beta_1^\dagger, \dots, \beta_\Omega^\dagger\} \subseteq \mathcal{N}_{\langle PQ\rangle}$.

$$\Upsilon_\# = \left[\Upsilon_\#^{PV}, \Upsilon_\#^{PQ} \right]^T$$

(4.6a)

$$\Upsilon_{\#}^{PQ} = \left[\Upsilon_{1,\#}^{\theta}, \dots, \Upsilon_{|\mathcal{N}_{\langle PQ\rangle}|,\#}^{\theta}, \Upsilon_{1,\#}^{V}, \dots, \Upsilon_{|\mathcal{N}_{\langle PQ\rangle}|,\#}^{V}\right]^{T} \tag{4.6b}$$

$$\Upsilon_{\downarrow,\#}^{PQ} = \mathrm{rank}_{\downarrow}\left(\mathrm{abs}(\Upsilon_{\#}^{PQ})\right) \tag{4.6c}$$

$$\Upsilon_{\downarrow,\#}^{PQ} = \left[\Upsilon_{\downarrow,1}^{PQ}, \dots, \Upsilon_{\downarrow,2\cdot|\mathcal{N}_{\langle PQ\rangle}|}^{PQ}\right]^{T} \tag{4.6d}$$

$$B^{\dagger} = \{(\beta_j^{\dagger}) : \beta_j^{\dagger} = \beta_i^{PQ} \,|\Upsilon_{i,\#}^{PQ} = \Upsilon_{\downarrow,j}^{PQ}, i \in \mathbb{N}[1, 2\cdot|\mathcal{N}_{\langle PQ\rangle}|], j \in \mathbb{N}[1, \Omega]\} \tag{4.6e}$$

where $\mathrm{rank}_{\downarrow}(\cdot)$ is a function that returns the descending rank of a generic vector, $\Upsilon_{\downarrow,\#}^{PQ}$ is the ranked criticality index, β_i^{PQ} corresponds to the buses that make up $\Upsilon_{\#}^{PQ}$, and $\beta_j^{\dagger}$ denotes the ranked buses.

From this process, the buses classified as the most effective for voltage stability support are typically contained in the same neighborhood of the bus responsible for driving the system to voltage collapse, leading to a concentrated actuation. However, BPSs usually contain more than one coherence area, i.e., a region of the system comprising buses with similar behavior, here denoted by the sets $\mathcal{Z}_r \subseteq \mathcal{N}$, where $r \in [1, \mho]$ indicates the area index and $\mho$ denotes the total number of areas. In this sense, bearing in mind that the voltage collapse is a local phenomenon, the characterization of the buses sensibility from a system-wide perspective in BPSs environments would not render the expected effect, as the centralized action in the system most critical region, $\mathcal{Z}_1$, would not produce meaningful improvements in other coherence regions, i.e. P-V$_\mathbb{G} \leftarrow \mathcal{Z}_r^{\dagger} \approx$ P-V$_\mathbb{G} \leftarrow \mathcal{Z}_r \,\forall\, r \neq 1$, where P-V$_\mathbb{G} \leftarrow \mathcal{Z}_r$ are representations of the system voltage stability when each respective coherence area $\mathcal{Z}_r$ assumes the condition to drive the system to voltage collapse; superscript † denotes the system response after system-wide based compensation. To obtain P-V$_\mathbb{G} \leftarrow \mathcal{Z}_r$ in case that the area under analysis is not the most critical region originally leading the system to voltage collapse, i.e., $\mathcal{Z}_r \,|r \neq 1$, compensations are performed in the more critical region(s) until the voltage collapse condition is shifted to the region $\mathcal{Z}_r$ of interest.

In this perspective, system-wide-based approaches would fail in case that a significant improvement in the system load margin is required. The realization of a large compensation would render a substantial increase in the voltage stability margin of the critical region, P-V$_\mathbb{G} \leftarrow \mathcal{Z}_1^{\dagger}$. However, under a system perspective, this action would only move the starting point of

voltage collapse to the subsequent most critical region, $\mathcal{Z}_r \,|\, r \neq 1$, which has not been improved by this compensation. This leads to an early saturation in the actual improvement capacity of the system voltage stability by the subsequent most critical-area voltage collapse condition, i.e., $\text{P-V}_\mathbb{G} \leftarrow \mathfrak{S}^\dagger = \text{P-V}_\mathbb{G} \leftarrow \mathcal{Z}_2^\dagger \,|\, \text{P-V}_\mathbb{G} \leftarrow \mathcal{Z}_2^\dagger \approx \text{P-V}_\mathbb{G} \leftarrow \mathcal{Z}_2$, where $\text{P-V}_\mathbb{G} \leftarrow \mathfrak{S}^\dagger$ depicts the actual system P-V curve after system-wide compensation. As a result, the system would most likely not be able to achieve the desired load margin improvement, ζ, where the respective lacking margin is denoted by χ.

This condition is depicted in Figure 4.1. It shows the voltage stability profile of a BPS with several coherence areas before and after the system-wide compensation. For this, the symbol $\wp_\mathbb{G}$ denotes the system operating point, and $\varepsilon\%$ is the required secure margin between the operative and voltage collapse points. This value is established by specific regulations as [2].
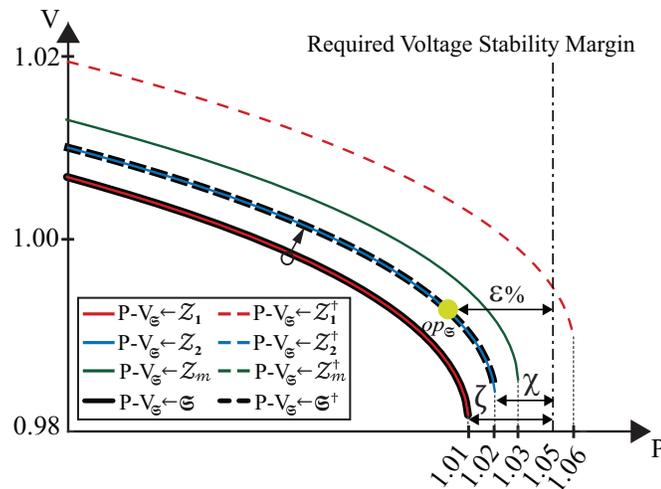
Figure 4.1: P-V curves for a system-wide approach

In this perspective, the development of voltage stability support strategies based on system-wide approaches may no longer be efficient to ensure safe operating conditions, as BPSs move toward new voltage stability requirements due to the increasing penetration of RESs. This new perspective requires a significant capacity for voltage stability margin improvement and the ability to effectively tackle constant shifts in the starting point of voltage collapse across different regions of the system. Seeking to accomplish these challenges and avoid the previously mentioned limitations, a second stage is developed based on the previous system-wide sensitivity. The proposed approach identifies local critical cores for voltage collapse and

divides the system into coherence areas denoted by the sets $\mathcal{Z}_r \subseteq \mathcal{N}$. The use of coherence areas is proven as an effective solution to improve voltage-related actions due to these phenomena local characteristics, e.g., disturbance propagation and security regions applications [19],[126], however, the proposed perspective and application have not yet been explored. The definition of critical cores avoids the centralized compensation performed by the system-wide approach, allowing a greater range for the system voltage stability margin improvement, ζ. Moreover, as compensation becomes distributed throughout the network, it is possible to continually tackle the development of voltage collapse even when a change in the region conducive to this incidence is imposed.

This feature is clearly shown in Figure 4.2. The proposed area-based strategy can improve all coherence areas voltage stability margin, i.e. $\text{P-V}_\mathbb{G} \leftarrow \mathcal{Z}_r^\ddagger \neq \text{P-V}_\mathbb{G} \leftarrow \mathcal{Z}_r \; \forall \, r \in [1, \mho]$. Therefore, allowing the achievement of the required/desired voltage stability margin improvement, $\zeta \in \mathbb{R} \,|\, \chi = 0$, even for scenarios demanding large improvements in the system loading margin. The system responses after the proposed area-based voltage stability support are denoted by the superscript $\ddagger$, respectively $\text{P-V}_\mathbb{G} \leftarrow \mathbb{G}^\ddagger$ and $\text{P-V}_\mathbb{G} \leftarrow \mathcal{Z}_r^\ddagger \; \forall \, r \in [1, \mho]$.
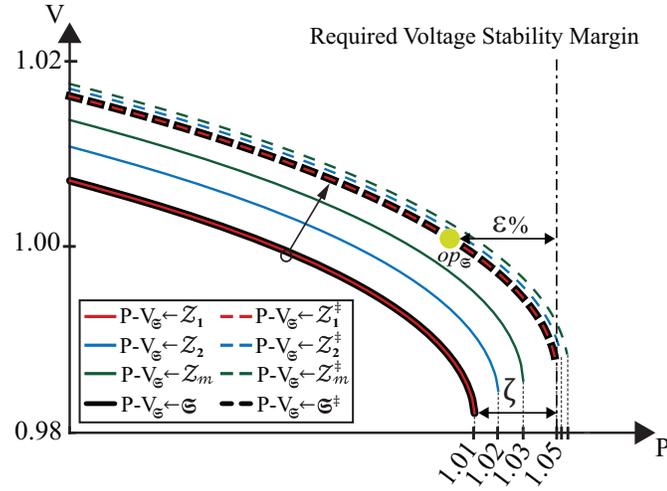
Figure 4.2: P-V curves for the proposed area-based approach

The initial step to divide the system into coherence areas is the definition of the first critical core, $\beta_1^\ddagger$, which is given by the system's most critical PQ-bus, i.e., $\beta_1^\ddagger = \beta_1^\dagger$. Following, based on the most critical location the neighbor buses belonging to the same area, $\mathcal{Z}_r$, are determined. For this, a scanning process is performed where the association of a candidate bus i is done if its normalized criticality index is greater than the partition parameter denoted by

$\varphi \in \mathbb{R}$, i.e., $\left(Y_i/Y_r^{\ddagger} > \varphi\right)$; and there exists an electrical connection $\{i,j\} \in \mathcal{V}$ between the candidate bus and the previously associated buses contained in the same area. Discussions about the determination of the partitioning parameter are omitted due to space constraints, the reader is referred to [31] where a comprehensive analysis is developed indicating that φ should be set within the range of 0.5 to 0.75. This process is performed for all but the $V\theta$ bus, $\mathcal{N}_{\langle V\theta \rangle}$, which is manually associated with the respective coherency area at the end of the process. Next, the respective buses collected in $\mathcal{Z}_r$ are extracted from the set of available buses for network partitioning and the process is repeated. After completing the first area division, the next critical core, $\beta_r^{\ddagger}$, is determined as the most effective PQ-bus that is not contained in the previous area(s) division and so on. This procedure is repeated until each bus is allocated in a respective area. The process that identifies the coherence areas $\{\mathcal{Z}_r, \forall\ r \in \mathbb{N}[1,\mho]\}$ around their respective critical cores $\{\beta_r^{\ddagger},\ \forall\ r \in \mathbb{N}[1,\mho]\}$, is described as follows:

$$Y_{r,\#}^{PQ} = \left[Y_{i,\#}^{\theta}, \ldots, Y_{\left|\mathcal{N}_r^{PQ}\right|,\#}^{\theta}, Y_{i,\#}^{V}, \ldots, Y_{\left|\mathcal{N}_r^{PQ}\right|,\#}^{V} \right]^{T}, \forall\ i \in \mathcal{N}_r^{PQ} \tag{4.7a}$$

$$Y_{r,\#}^{\ddagger} = \max\left(\mathrm{abs}\left(Y_{r,\#}^{PQ}\right)\right) \tag{4.7b}$$

$$\mathcal{Z}_r = \left\{\left(\beta_r^{\ddagger}\right): \beta_r^{\ddagger} = \beta_i^{PQ} \left| Y_{i,\#}^{PQ} = Y_{r,\#}^{\ddagger}, i \in \mathbb{N}\left[1, 2 \cdot \left|\mathcal{N}_{\langle PQ\rangle}\right|\right]\right.\right\} \tag{4.7c}$$

$$\mathcal{Z}_r = \left\{\left(\beta_i\right): Y_{i,\#}/Y_{r,\#}^{\ddagger} > \varphi,\ i \in \mathcal{V}\left|_{\mathcal{Z}_r}, i \in \mathbb{N}\left[1, \left|\mathcal{N}_{\langle PV\rangle}\right| + 2 \cdot \left|\mathcal{N}_{\langle PQ\rangle}\right|\right]\right.\right\} \tag{4.7d}$$

$$\mathcal{N}_{r+1}^{Sys} = \mathcal{N}_r^{Sys} \backslash \mathcal{Z}_r \tag{4.7e}$$

$$\mathcal{N}_{r+1}^{PQ} = \mathcal{N}_r^{PQ} \backslash \mathcal{N}_{r+1}^{Sys} \tag{4.7f}$$

where $\mathcal{N}_r^{Sys}$, $\mathcal{N}_r^{PQ}$ and $Y_{r,\#}^{PQ}$ respectively denote the sets of all buses, PQ-buses, and criticality index of flexible PQ-buses that are not associated with any area. $Y_{r,\#}^{\ddagger}$ represents the criticality index of the critical core $\beta_r^{\ddagger}$. $\mathcal{Z}_r$ represents the buses collected in a respective coherence area $r \in \mathbb{R}$, while β_i denotes the bus corresponding to the criticality index $Y_{i,\#}$. The initial conditions are given by $\mathcal{Z}_1 = \emptyset$, $\mathcal{N}_r^{Sys} = \mathcal{N}$, $\mathcal{N}_1^{PQ} = \mathcal{N}_{\langle PQ\rangle}$. The respective set collecting all critical cores

is defined by $B^{\ddagger} = \{\beta_1^{\ddagger}, \dots, \beta_{\mho}^{\ddagger}\} \subseteq \mathcal{N}_{\langle PQ \rangle}$.

By using the critical cores and coherence areas knowledge, a novel area-based voltage stability index is obtained for each bus. This index, denoted by $\Psi_{i,\langle \nabla \rangle}^{\ddagger}$, is composed of two terms. The first term represents the area's contribution based on the density of critical spots, while the second term denotes the respective contribution from the bus based on its criticality information. This means that if one area has a very critical location prone to voltage collapse but possesses a low density of critical buses, the total compensation in this area will not be performed in excess, as compensating this very critical spot renders an overall improvement of the area's voltage stability. On the contrary, if an area has a high density of critical points, additional compensation will be required, as the compensation of the single most critical location will not lead to an actual improvement of the area voltage stability profile. The proposed index $\Psi_{i,\langle \nabla \rangle}^{\ddagger}$ and the flexibility contribution of each bus, denoted by the set $\Psi_{\langle \nabla \rangle}^{\ddagger}$, are represented by the following equations.

$$Y_{r,\langle \nabla \rangle} = \{(Y_{i,\langle \nabla \rangle}) : Y_{i,\langle \nabla \rangle} = Y_{i,\#}/Y_{r,\#}^{\ddagger}, \beta_i \in Z_r, i \in \mathbb{N}[1, \Gamma_r], r \in \mathbb{N}[1, \mho]\} \tag{4.8a}$$

$$\Psi_{r,\langle \nabla \rangle}^{\ddagger} = \left\{(\Psi_{i,\langle \nabla \rangle}^{\ddagger}) : \Psi_{i,\langle \nabla \rangle}^{\ddagger} = \left(\frac{\|Y_{r,\langle \nabla \rangle}\|}{\sum_{M=1}^{\mho}\|Y_{M,\langle \nabla \rangle}\|} \cdot \frac{Y_{i,\langle \nabla \rangle}}{\sum_{I=1}^{\Gamma_r} Y_{I,\langle \nabla \rangle}}\right)\right. \tag{4.8b}$$

$$Y_{i,\langle \nabla \rangle} \in Y_{r,\langle \nabla \rangle}, i \in \mathbb{N}[1, \Gamma_r], r \in \mathbb{N}[1, \mho]\}$$

$$\Psi_{\langle \nabla \rangle} = \{\Psi_{r,\langle \nabla \rangle}^{\ddagger} \cdot \Lambda, \dots, \Psi_{\mho,\langle \nabla \rangle}^{\ddagger} \cdot \Lambda\}, r \in \mathbb{N}[1, \mho] \tag{4.8c}$$

where $Y_{i,\langle \nabla \rangle}$ represents the criticality of a generic bus $i \in \mathbb{R}$, Γ_r is the number of buses used for compensation in area $r \in \mathbb{R}$, $Y_{r,\langle \nabla \rangle}$ and $\Psi_{r,\langle \nabla \rangle}^{\ddagger}$ are sets containing the buses criticality and proposed index of a respective area $r \in \mathbb{R}$, and Λ represents the total system flexibility usage, i.e., $\sum_{i \in \mathcal{N}_{\langle L \rangle}} P_{\langle DR \rangle_i} + P_{\langle DG \rangle_i} + P_{\langle EV \rangle_i} = \Lambda$.

A detailed description of the process to obtain the proposed area-based voltage stability index is illustrated in Figure 4.3.
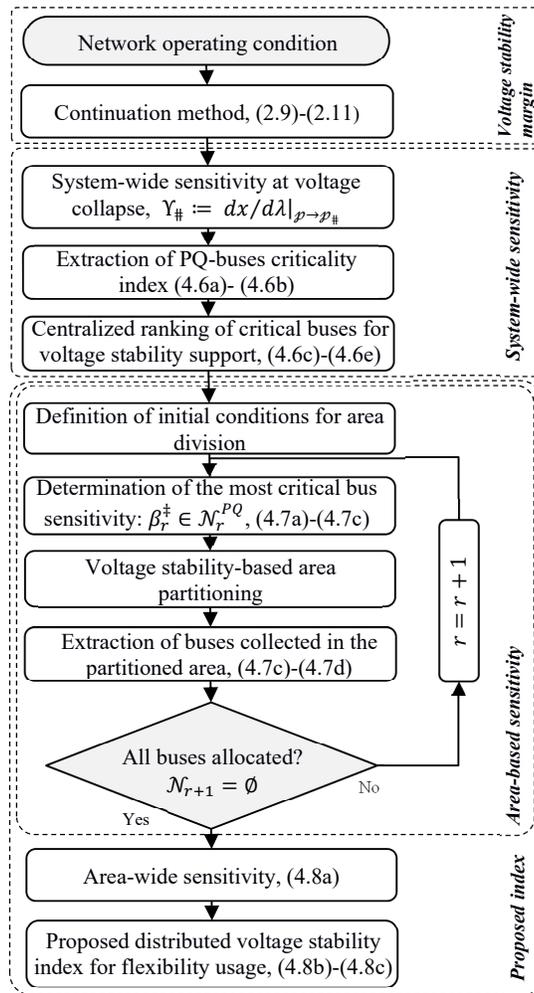
Figure 4.3: Proposed methodology description

4.5 Results

This section depicts the requirement for area-based voltage stability support as BPSs move toward large penetration of RESs. Here, comparative case studies are developed to showcase the improvements provided by the proposed approach for modern BPSs' voltage stability support, in contrast to traditional direct system-wide strategies and successive linear programming (SLP). For this purpose, case studies are developed employing the IEEE 118-bus system [118] modified to represent grid developments, where BPSs are likely to experience operating conditions close to their limits with an increase in RESs penetration. The system load is doubled in comparison with the base case, and a total of 20 p.u. of additional wind generation are eventually distributed on buses as described in Table 4.2. In this analysis, a conservative

case study is employed. Loads are modeled as constant power so that voltage reductions would not improve the system voltage stability capacity, and a unity power factor is assumed for FRs such that the reactive power consumption is maintained at the nominal level. In this configuration, the system operates with a voltage stability margin of 108% surpassing the Western Electricity Coordinating Council (WECC) minimum requirement of 105% [2]. In this standard, the current system operative condition is denoted by $p_{\mathbb{G}}$ represents the system loading margin at 100%. The requirement for an additional 5% stability margin, $\varepsilon = 5\%$, is an industrial standard that seeks to accommodate possible unpredicted load variations adopted by several system operators worldwide.

Table 4.2: RESs placement

Allocation of RESs (buses)								
106	108	101	79	78	118	43	35	37

Owing to RESs lack of guaranteed power contribution, scenarios with low generation states can meaningfully affect the system voltage stability margin and even lead the system to operating conditions beyond the voltage stability limit. This scenario requires effective voltage support actions to ensure a reliable system operation, which is explored by the performed case studies considering FRs usage to ensure secure voltage stability margins in the absence of RESs contribution. In this perspective, three main case studies are developed to demonstrate the proposed approach's effectiveness: 1) Validation and performance evaluation; 2) Sensitivity analysis; and 3) Comparative analysis between FRs and RESs operating under voltage control for voltage stability support.

4.5.1 Validation and performance evaluation

The first case study highlights modern BPSs' significant need for voltage stability support and the superior ability of the proposed area-based approach to deal with the new system operative reality and requirements. For this, comparisons with a traditional direct system-wide approach and SLP [127] are performed. The comparative system-wide approach is based on the sensitivity of the tangent vector. This technique is proposed in [31] and employed in [4] to determine the set of candidate buses for voltage stability support. For this, four sub-cases are developed, respectively: Case 1 - System behavior without voltage stability support; Case 2 - System behavior with FRs support based on traditional direct system-wide

strategy; Case 3 - System behavior with FRs support based on the proposed direct area-based voltage stability index; Case 4 - System behavior with FRs support based on successive linear programming.

The respective voltage stability profile of the system for Cases 1-3 are depicted in Figure 4.4(a)-(b), where P-$V_\mathbb{G} \leftarrow \mathbb{S}$ depicts the actual system P-V curve, P-$V_\mathbb{G} \leftarrow Z_r$ are representations of the system voltage stability when each respective coherence area Z_r assume the condition to drive the system to voltage collapse. The system responses without voltage stability support (Case 1) are denoted by the representations without superscript, while the system behavior after the provision of voltage stability support based on system-wide (Case 2) and the proposed area-based approach (Case 3) are respectively denoted by the superscripts † and ‡; $p_\mathbb{G}$ indicates the system operating condition, ζ describes the necessary improvement in the system loading margin and χ represents the residual voltage stability margin to ensure the system operates within the established limits by regulation. In this system, nine buses are used for FR support, and three coherence areas are defined.
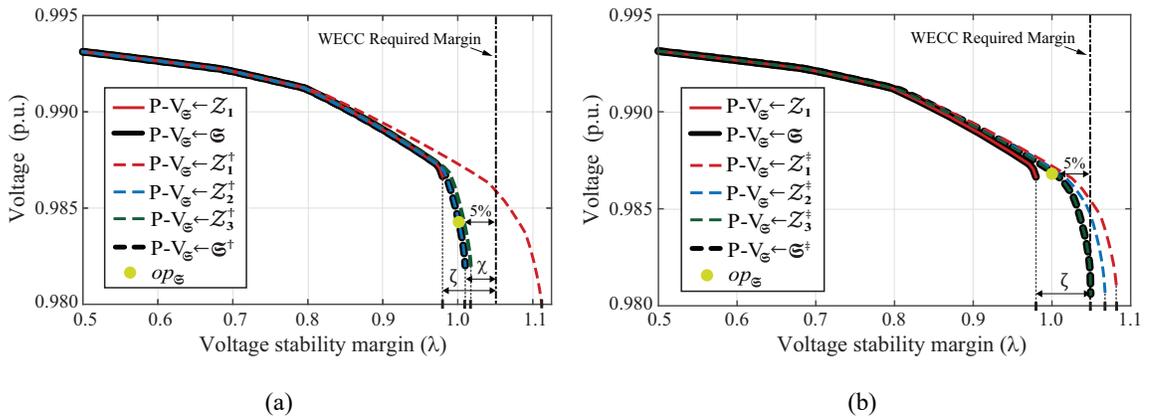
Figure 4.4: P-V curves for the system before and after voltage stability support based on (a) system-wide strategy;(b) proposed area-based index

Figure 4.4(a) depicts the system behavior for Cases 1-2. Based on Figure 4.4(a), one can conclude about the system requirement for voltage stability support, changes in the critical region that lead the system to voltage collapse, and the consequent inability of the system-wide approach to achieving large improvements in the system load margin. Analyzing Figure 4.4(a), one may observe that the most critical region P-V curve for Case 1, i.e., when the dispatchable generators provide the network's expected RES generation and no action is taken to improve the system voltage stability margin, P-$V_\mathbb{G} \leftarrow Z_1$ represents the actual overall system voltage

stability margin, $P\text{-}V_\mathbb{G} \leftarrow \mathbb{G} = P\text{-}V_\mathbb{G} \leftarrow \mathcal{Z}_1$. In this scenario, although the power/demand balance can be achieved, the system would experience voltage collapse, as the system loading margin denoted by $\lambda=0.98 \mid P\text{-}V_\mathbb{G} \leftarrow \mathbb{G}$, is lower than the actual demand requirement, $\wp_\mathbb{G} = 1.00$. In this sense, actions must be taken to improve the system voltage stability to ensure the required secure operating condition of $\lambda=1.05$. To achieve this goal, an improvement of 7% in the system load margin is necessary, i.e., $\zeta = 7\%$. In this sense, first, FRs are used to provide voltage stability support based on a system-wide perspective.

As one may observe, the system-wide strategy can significantly enhance the voltage stability margin of the originally most critical region of the system to $\lambda=1.11 \left| P\text{-}V_\mathbb{G} \leftarrow \mathcal{Z}_1^\dagger \right.$, however, this improvement is not translated to the overall system stability margin expressed by $P\text{-}V_\mathbb{G} \leftarrow \mathbb{G}^\dagger$. The centralized actuation in the most critical buses is not able to improve other regions voltage stability, $P\text{-}V_\mathbb{G} \leftarrow \mathcal{Z}_r^\dagger \approx P\text{-}V_\mathbb{G} \leftarrow \mathcal{Z}_r, \forall\, r \neq 1 \mid r \in \mathbb{N}[1,3]$. In contrast, it leads to the overcompensation of the previously most critical region of the system, $\mathcal{Z}_1$, leading to the change of the location responsible to drive the system to voltage collapse to the next most critical region, i.e., $\mathcal{Z}_2$. Therefore, limiting the system voltage stability margin improvement by the subsequent most critical area voltage collapse condition, $P\text{-}V_\mathbb{G} \leftarrow \mathbb{G}^\dagger = P\text{-}V_\mathbb{G} \leftarrow \mathcal{Z}_2^\dagger$, which did not have its load margin significantly affected by the performed compensation, i.e., $P\text{-}V_\mathbb{G} \leftarrow \mathcal{Z}_2^\dagger \approx P\text{-}V_\mathbb{G} \leftarrow \mathcal{Z}_2$. In this perspective, the system improved stability margin after voltage stability support based on system-wide perspective is denoted by $\lambda=1.01 \mid P\text{-}V_\mathbb{G} \leftarrow \mathbb{G}^\dagger$. The obtained condition is still lower than the WECC safe operating margin criteria of 105%, remaining 4% of the required voltage stability margin to be fulfilled, i.e., $\chi = 4\%$. This result would inevitably demand costly system expansions and the installation of new infrastructures to reach the regulation criteria [2].

Seeking to fulfill the secure voltage stability margin requirement and avoid costly system upgrades, the proposed area-based voltage stability index is employed, being the results depicted in Figure 4.4(b). From Figure 4.4(b) one can observe that the FRs usage based on the proposed area-based approach leads to an overall improvement in the system voltage stability margin. In this scenario, all system coherence areas have achieved the voltage stability margin requirement by WECC, i.e., $\lambda \geq 1.05 \left| P\text{-}V_\mathbb{G} \leftarrow \mathcal{Z}_r^\ddagger \,\forall\, r \in \mathbb{N}[1,3] \right.$. As well, after performed the proposed area-based voltage stability support, the system most critical region is shifted to the coherence area $\mathcal{Z}_3$, $P\text{-}V_\mathbb{G} \leftarrow \mathbb{G}^\ddagger = P\text{-}V_\mathbb{G} \leftarrow \mathcal{Z}_3^\ddagger$. However, differently from the system-wide strategy, the proposed approach distributed action in the network critical cores can satisfactorily

address this issue, overcoming the early saturation faced by the system-wide strategies and leading to a system voltage stability margin of $\lambda=1.05 \left| \text{P-V}_\mathbb{G} \leftarrow \mathbb{S}^\ddagger \right.$. The obtained results are due to the distributed actions in the network most critical cores, which allows for a greater range of improvement to the system voltage stability margin, ensuring the required load margin improvement of $\zeta=7\%|\chi=0$ with a flexibility usage of $\Lambda= 2.5$ p.u..

Following, a new case study is developed seeking to verify the proposed direct approach ability to determine the system most adequate allocation for FRs support in comparison with SLP. The obtained results present significant similarity between the proposed direct approach and SLP, i.e., 67% of the selected buses for FRs usage are common for both methods. Moreover, an equivalent level of voltage stability margin improvement is achieved by both methods using the same amount of flexibility, i.e. $\lambda=1.05$ for both Case 3 and Case 4 with a flexibility usage of $\Lambda= 2.5$ p.u. These results showcase the proposed direct approach's ability to meaningfully improve the system load margin at a significantly reduced computational cost. Eliminating the computational burn imposed by the successive iterations necessary for gathering feedback information required by optimization technics.

A summary of the system voltage stability margin is presented for Cases 1-4 in Table 4.3. The respectively selected buses and their flexibility usage for Cases 2-4 are shown in Table 4.4, where the totaling of all buses' flexibility usage for each case study in Table 4.4 must be equal to the total amount of flexibility usage defined by Λ.

Table 4.3: Voltage stability margin for different case studies

	Load margin	Max. Load (p.u.)	Λ (p.u.)
Case 1	0.98	72.9[a]	-
Case 2	1.01	75.1	2.5
Case 3	1.05	78.0	2.5
Case 4	1.05	78.3	2.5

[a] $\mathscr{p}_\mathbb{G} = 74.4$ p.u.

Table 4.4: Flexibility usage outlook for Λ=2.5 p.u.[a]

Case 2: Traditional system-wide method								
Bus	109	108	106	101	94	102	95	93	86
$\Psi_{i,\langle \nabla \rangle}$ (p.u.)	0.53	0.51	0.46	0.19	0.17	0.17	0.16	0.16	0.15
Case 3: Proposed area-based index, $\Gamma_r=3, \forall\, r \in \mathbb{N}[1,3]$								
Bus i	109	108	106	41	39	44	33	35	117
$\Psi_{i,\langle \nabla \rangle}$ (p.u.)	0.29	0.28	0.25	0.29	0.29	0.22	0.29	0.29	0.29
Case 4: Successive Linear Programming								
Bus i	109	108	106	41	39	117	2	3	13
$\Psi_{i,\langle \nabla \rangle}$ (p.u.)	0.25	0.24	0.21	0.53	0.35	0.24	0.32	0.21	0.07

[a] $\varphi_{\langle flex \rangle_i} \cdot P_{\langle L \rangle_i} = \Psi_{i,\langle \nabla \rangle}$

4.5.2 Sensitivity analysis

In this section, sensitivity analyses are performed to investigate the influence of loads uncertainty and FRs' usage impact on the system voltage stability margin. The performed case studies present global system sensitivities, seeking to highlight the proposed method's capability to meet secure voltage stability margins, prevent early saturation, and significantly improve the system voltage stability margin range.

First, the impact of load uncertainty is addressed by featuring load scenarios extracted from [65]. These case studies denoted as S1, S2, and S3 represent the system loading for 98%, 100%, and 102%, respectively. Obtained results indicate that the proposed approach can satisfactorily address loads uncertainty without prejudice to the guarantee of secure voltage stability margin. In all analyzed case studies, the necessary range of improvement is met, i.e., there is no remaining voltage stability margin to be fulfilled, $\chi = 0\%$. The flexibility usage for each scenario is respectively, S1: $\zeta = 5\%|\ \Lambda = 1.5$ p.u.; S2: $\zeta = 5\%|\ \Lambda = 2.5$ p.u.; and S3: $\zeta = 5\%|\ \Lambda = 4.0$ p.u.. A detailed description of each bus contribution is presented in Table 4.5.

Table 4.5: Flexibility usage for an operational outlook considering loads uncertainty

Bus $\Psi_{i,\langle \nabla \rangle}$ (p.u.)	109	108	106	101	94	102	95	93	86	Λ (p.u.)
S1	0.18	0.17	0.15	0.18	0.17	0.13	0.17	0.17	0.17	1.5
S2	0.29	0.28	0.25	0.29	0.29	0.22	0.29	0.29	0.29	2.5
S3	0.47	0.45	0.41	0.47	0.46	0.35	0.47	0.47	0.46	4.0

Next, the sensitivity of voltage stability margin concerning FRs usage is investigated and illustrated in Figure 4.5. For this, a strategy similar to the one presented in [66] is employed, in which successive variations in the use of flexibility are performed and the voltage stability margin of the system is analyzed. As one may observe, the proposed approach sustains significant improvements in the system voltage stability margin with the increasing usage of flexibility. Moreover, a large improvement in the operational range is verified. This result is expected given the proposed area-based index distributed action in the network critical cores. In this perspective, all system coherence areas are compensated considering the criticality of the respective region, therefore avoiding the overcompensation in a single region and the consequent inefficiency in the overall improvement of system voltage stability margin. For comparison's sake, a traditional system-wide approach is presented, where one can observe a

rapid saturation with a flexibility usage of $\Lambda=0.4$ due to its centralized compensation in the most critical buses.

In addition, it should be noted that local voltage stability sensitivity metrics are embedded in the proposed approach to defining the respective candidate buses. In this sense, the selected buses for FR usage depicted in Table 4.4, represent the system's most locally sensible buses under-voltage stability perspective.
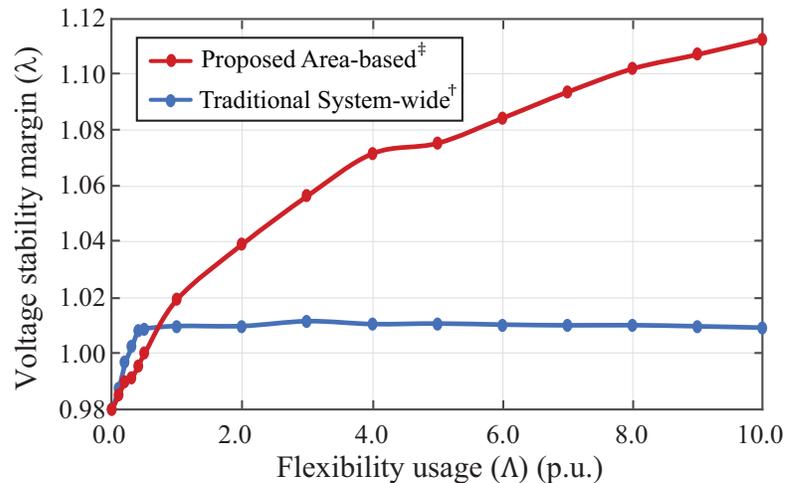
Figure 4.5: Sensitivity of voltage stability margin for different flexibility usage levels

4.5.3 Flexible resources and RES operating under voltage control

This section seeks to assess FRs' ability to improve voltage stability in comparison, and association, with RES generation under voltage control. Different FRs are considered, including dispatchable DGs of rated power {15,8,10,14} MVA connected in buses {109,108,41,33}; EVs with level 2 chargers presenting charging/discharging capacity of 11 kW associated in the respective amounts, i.e. number of EVs, {250, 250, 380; 330, 460, 290, 150, 240, 190} at selected buses for flexibility support, i.e. buses {109, 108, 106, 41, 39, 44, 33, 35 117}; as well as DR capacity as necessary. The dispatch of FRs is based on priority rank seeking to maximize demand supplying, i.e., DGs are the first to be used, followed by EVs, and in case that additional flexibility is necessary DR is applied. Given the chapter goal of improving power systems voltage stability, renewables operating under voltage control have their reactive power focused on load margin enhancement [128], i.e., $\mathcal{F}^{\circ} = \lambda - C_v \cdot \left[\sum_{\forall i} \max\left(0, |V_i| - \overline{V}\right) + \right.$

$\sum_{\forall i} \max(0, |V_i| - \underline{V})]$, where each unit has the following local setting $Q_i = \text{Constr}\Big(\hat{Q}_i + \alpha_i^\diamond \cdot \Delta P_i,$

$\sqrt{\overline{S_i}^2 - (\hat{P}_i + \Delta P_i)^2}\Big)|V_i \leq \overline{V}$, $\quad \text{Constr}(\mathfrak{x}, \overline{\mathfrak{x}}) = \left\{\mathfrak{x}, |\mathfrak{x}| \leq \overline{\mathfrak{x}}; \left(\frac{\mathfrak{x}}{|\mathfrak{x}|}\right) \cdot \overline{\mathfrak{x}}, otherwise\right\}$, where $\mathcal{F}^\diamond$

denotes the objective function, C_v is the penalty term for voltage violation, $\overline{V}$ and $\underline{V}$ denote the maximum and minimum operational voltage limits, $\overline{S_i}$ is the unit rated power capacity, $\alpha_i^\diamond$ is the slope coefficient and $\hat{Q}_i$ and $\hat{P}_i$ are reactive and active power setpoints.

Here three comparative case studies are presented: 1) RESs operating under voltage control, $\mathfrak{S}^*$; 2) Sole use of FRs, $\mathfrak{S}^\ddagger$; 3) Combined use of FRs and RESs operating under voltage control, $\mathfrak{S}^{*,\ddagger}$. The respective results are depicted in Figure 4.6.
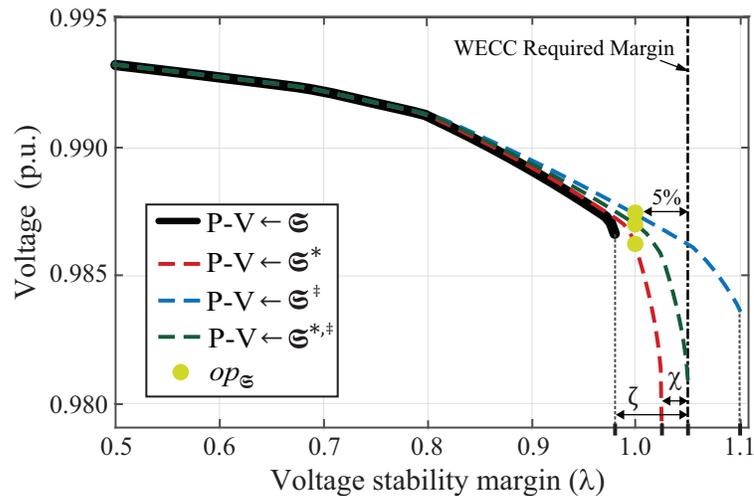
Figure 4.6: Comparative analyses of voltage stability margin considering renewables operation under voltage control and FR

As one may observe, RESs operation under voltage control can improve the system load margin up to 103% using a combined total of 8.3 p.u. Still, their contribution is not sufficient for ensuring the necessary secure load margin established by WECC regulation, i.e., 105%. This perspective is significantly enhanced considering the use of FRs. As depicted by P-V ← $\mathfrak{S}^\ddagger$ in Figure 4.6, with the same 8.3 p.u. of FRs usage, one can achieve a system voltage stability margin of 110%. This result significantly surpasses WECC operational requirements and represents an improvement of 42% in comparison with RESs support. Demonstrating that FRs are more effective than RESs operating under voltage control to improve the system voltage stability. These results are expected as FRs' dispatch are performed from the system most

critical buses under-voltage stability perspective, whereas RESs contributions are conditioned to the location of the unit installation. These locations are typically subjected to the availability of potential capacity for the respective development, e.g., wind generators, and may not be the most adequate location for voltage stability support.

Still, a combined operation of RESs under voltage control and FRs can significantly improve the system voltage stability and lead to more efficient use of FRs. In this case, RESs action takes priority over FRs, which are used to fulfill the remaining gap to ensure secure voltage stability margins. This combined operation leads to meaningful benefits as FRs usage is significantly reduced. A comparison with Case 2 in Section 4.1 indicates that by combining the use of FRs and RESs under voltage control, a reduction of 56% in the total application of FRs is achieved. Moreover, this reduction represents a decrease of 73% in DR usage when considering multiple sources of flexibility, which can significantly avoid possible curtailments requirements. The detailed load margin is illustrated by P-V $\leftarrow \mathfrak{S}^{\ddagger}$ in Figure 4.6, while the contribution of each group is depicted in Table 4.6.

Table 4.6: Individual contributions for combined operation of FRs and RESs under voltage control for voltage stability margin improvement

RES	Bus i	106	108	101	79	78	118	43	35	37
	$Q_{\langle G \rangle}$ (p.u.)	1.5	1.0	0.7	0.4	1.5	1.4	0.2	0.5	1.1
Flexible resources	Bus i	109	108	106	41	39	44	33	35	117
	$\Psi_{i,\langle \nabla \rangle}$ (p.u.)	0.13	0.12	0.11	0.13	0.13	0.1	0.13	0.13	0.13
	DGs	100%	67%	-	77%	-	-	100%	-	-
	EVs	-	33%	76%	23%	78%	64%	-	41%	32%
	DR	-	-	24%	-	22%	36%	-	59%	68%

4.6 Summary

Traditional methods may no longer be efficient for securing safe voltage stability margins for BPSs moving toward large penetration of intermittent RESs. In this chapter, a novel area-based outlook using FRs is proposed to tackle this new BPS perspective. The proposed approach can overcome the early saturation in the improvement of the BPS voltage stability margin faced by traditional centralized strategies that may endanger the achievement of secure operative conditions for modern BPSs. For this, the system's most critical cores and their respective coherence areas are identified. Based on this information a novel distributed voltage stability index is developed. The results indicate that the application of the proposed index to

identify effective buses for voltage support and their respective ability to increase the system load margin, in association with FRs, can greatly improve and secure safe static voltage stability margins. The main contributions of this work can be summarized as follows:

- Proposal of a novel area-based voltage stability index considering BPS coherence areas and critical cores.

- Development of a new outlook for voltage stability support of modern BPS based on FRs.

- Prevention of early saturation in improving the overall system voltage stability margin due to centralized overcompensation.

- Significant enhancement of BPS voltage stability margin range, a critical condition for a BPS with large penetration of intermittent RESs generation.

Chapter 6:   Conclusion

6.1 Context

In Chapter 6, the results, contributions of this thesis presented in Chapters 3-5 are summarized. Then, future research directions are provided based on this work.

6.2 Contribution Summary and Conclusions

The research topics in this thesis present new methods and analysis to tackle operation and stability challenges in face of the BPS modernization with high penetration of DERs. The contribution of each chapter is summarized as follows.

In Chapter 3, the main contribution is characterized by capitalizing on the proposed network partitioning based on coherent areas of voltage stability the ability to enhance SSRs with high penetration of RES. In this sense, the main improvements are listed as follow:

- Improvement of the system criticality index determination considering WAMS using PMU: The precise measurements of the system operating conditions provided by WAMS using PMU can meaningfully aid the process for calculating their energy function-based criticality index, in special for the LVS determination. This significantly improves this process, enabling its application for the development of proposed network partitioning in the short-term.

- Novel energy function-based network partitioning considering high precision measurements: Based on the system energy function-based criticality, a new network partitioning algorithm is proposed. This method is unlike the traditional approaches that achieve network partitioning considering the construction of a cluster of buses with similar sensitivity. The proposed method directly identifies the boundaries of the coherence areas in a way that changes in the system states tracked by WAMS using PMU can render the adjustment of the boundaries of the partitioned region, leading to the adaptive definition of the system coherence areas.

- Adaptive SSR construction based on coherent areas of static voltage stability: The proposed partitioning method enables the adaptive definition of generator groups

applied to SSR. This feature allows for mitigating the effects of variation of the system operating conditions, such as those resulting from RESs intermittency, in a way that operating conditions previously deemed unsafe by the traditional SSR evaluation can become operational without the need for additional infrastructures or systems' expansions.

In Chapter 4, the main contribution is characterized by capitalizing on FRs the ability to improve voltage stability margin. In this sense, the main improvements are listed as follow:

- New outlook for voltage stability support of modern BPS based on FRs: the proposed area-based design enables the distributed potential of FRs to fulfill the sounding requirements of modern BPS voltage stability. Different from other approaches that would require new infrastructures or detract from the original design of the existing explored system, e.g., HVDC, wind, and solar-based applications, FRs are meant for this kind of requirement.

- Prevention of early saturation in voltage stability margin improvement: The identification of critical cores and system partitioning allows the proposed index to determine the most effective buses for voltage stability support along with different coherent areas of the network. This feature enables the system to avoid centralized actions in a single region, which in case of a change in the critical location driving the system to voltage collapse would prevent local overcompensation and the early saturation in the overall system load margin improvement.

- Enhancement of BPS voltage stability margin range: The proposed approach's above-mentioned ability to prevent early saturation allows for substantial increases in voltage stability support actions to be converted into continuous improvements in the system voltage stability margin. This is a critical aspect for systems with broad participation of intermittent RESs that might not be achieved with system-wide based solutions, due to possible overcompensation in a specific region as large voltage stability support actions yield to changes in the most critical location prone to voltage collapse.

6.3 Relevance for Industry and Socioeconomic Welfare

The pursue of socioeconomic welfare is a fundamental aspect of the development of society. This perspective is characterized by the conceptualization and development of activities

in ways that can simultaneously satisfy individual's and society's material and non-material needs. It leads to better living conditions for individuals under multiple societal levels, e.g., local, state, national and society.

In this sense, the application of products generated by research projects can have implications that go beyond their technical expertise. Thus, it is fundamental that these applications are subjected to ethical conduct evaluation, where a responsible decision-making process must consider how the work affects the safety, health and welfare of the society and environment, rejecting corrupted principles and avoiding conflicts of interest.

Given electricity critical participation as an enabling factor for multiple society activities, e.g., water treatment, food processing, transportation, health care, thorough planning is necessary to guarantee its reliable supply while achieving socioeconomic welfare. Considering modern EPSs evolving generation matrix, the traditional electricity generation model has been challenged and a significant opportunity is presented to improve its socioeconomic welfare given the large potential for diversity in the generation resources mix and possible regionalization of generation through significant participation levels of DERs. Brazil is currently among the leaders in the overall rank of RESs generation, with a very large potential for further resource exploration. Still, while the penetration of RESs provides meaningful benefits under environmental aspects. They introduce significant challenges that must be overcome by BPS operators, to ensure the expected reliability in electricity supply, as well as quick restoration of electricity service when facing major disruptive events, e.g., natural disasters caused by wildfires and hurricanes, without jeopardizing social welfare.

In this perspective, the study of solutions that can go beyond that provision of sufficient conditions to the integration of RESs in the BPS, but that can also provide opportunities to effectively harness these resources potential to support multiple BPS operational aspects, i.e., DERs and MGs, participation on operation and stability of BPS, are urgently necessary.

6.4 Publications to-date

Journal

J1) **MONTEIRO, M. R.**; RODRIGUES, Y. R.**;** ABDELAZIZ, M.; WANG, L.; SOUZA, A. C. Z., "Area-Based Voltage Stability Support Using Flexible Resources," *Electr. Power Syst. Res.*, vol. 186, Sep. 2020, Article 106384.

J2) MONTEIRO, J. R.; RODRIGUES, Y. R.; **MONTEIRO, M. R.**; SOUZA, A. C. Z.; FULLY, I. L.; "Intelligent RMPS Allocation for Microgrids Support during Scheduled Islanded Operation," *IEEE Access*, vol. 8, pp. 117946-117960, Jun. 2020.

J3) **MONTEIRO, M. R.**; ALVARENGA, G. F.; RODRIGUES, Y. R.; SOUZA, A. C. Z.; LOPES, B. I. L.; PASSARO, M.; ABDELAZIZ M., "Network partitioning in coherent areas of static voltage stability applied to security region enhancement," *Int. J. Electr. Power Energy Syst*, vol. 117, May 2020, Article 105623.

J4) RODRIGUES, Y. R.; **MONTEIRO, M. R.**; ABDELAZIZ, M.; WANG, L.; SOUZA, A. C. Z.; RIBEIRO, PAULO F.; "Improving the Autonomy of Islanded Microgrids Through Frequency Regulation," *Int. J. Electr. Power Energy Syst.*, vol. 115, Feb. 2020, Article 105499.

Conference

C1) **MONTEIRO, M. R.**; RODRIGUES, Y. R.; MINAMI, J. P. O. S.; SOUZA, A. C. Z.; RIBEIRO, P. F.; BONATTO, B. D.; WANG, L.; EBERLE, W., "Unbalanced Frequency Dependent Load Flow for Microgrids," IEEE PES General Meeting, Portland, 2018.

C2) RODRIGUES, Y. R.; **MONTEIRO, M. R.**; SOUZA, A. C. Z.; RIBEIRO, P. F.; WANG, L.; EBERLE, W., "Adaptative Secondary Control for Energy Storage in Island Microgrids," IEEE PES General Meeting, Portland, 2018.

Book Chapters

B1) **MONTEIRO M. R**., RODRIGUES, Y. R**.**; ZAMBRONI DE SOUZA, A. C.; RIBEIRO, P. F., "PSO Applied to Reactive Power Redispatch for Loss Reduction Considering Renewable Generation," Decision Making Applications in Modern Power Systems, 1ed. Elsevier, 2020, pp. 247-267.

B2) **MONTEIRO M. R**., RODRIGUES, Y. R**.**; ALVARENGA G. "Considerations on Microgrids Operation and Stability," Integration of Renewables and Intelligent Electrical Networks, 1ed. Rio de Janeiro: Interciência, 2020. – Portuguese.

B3) **MONTEIRO M. R**; SOUZA, A. C. Z.; RIBEIRO, P. F. "Modeling and Harmonic Analysis for Determining the Occupational Pattern: Case Study for a University Environment with Renewable Sources," Smart Cities and Smart Grids in a multidisciplinary perspective. 1ed. Rio de Janeiro: Interciência, 2018. – Portuguese.

6.5   Directions for Future Works

In continuation of this work, the following topics are suggested as future works:

1) Expansion of the proposed methods to include uncertainty of variable RESs and calculate associated risks.
2) Inclusion of regulation and marketing policies that can assure BPS reliability.
3) Optimal allocation of mobile power resources to improve the load restoration process.
4) Development of a new algorithm to enable the different stages of the restoration process.

References

[1] D. Marujo, A. C. Zambroni de Souza, B. I. L. Lopes, M. V. Santos, and K. L. Lo, "On control actions effects by using QV curves," *IEEE Trans. Power Syst.*, vol. 30, no. 3, pp. 1298-1305, May 2015.

[2] Guide to WECC/NERC planning standards I.D: Voltage support and reactive power, RRWG and WECC, Mar. 2006.

[3] J. Liu, Y. Xu, Z. Y. Dong, and K. P. Wong, "Retirement-driven dynamic VAR planning for voltage stability enhancement of power systems with high-level wind power," *IEEE Trans. Power Syst.*, vol. 33, no. 2, pp. 2282–2291, Mar. 2018.

[4] A. C. Zambroni de Souza, L. M. Honório, and G. L. Torres, "Increasing the loadability of power systems through optimal-local-control actions," *IEEE Trans. Power Syst.*, vol. 19, no. 1, pp. 188–194, Feb. 2004.

[5] M. Bakhtvar, and A. Keane, "Allocation of wind capacity subject to long term voltage stability constraints," *IEEE Trans. Power Syst.*, vol. 31, no. 3, pp. 2404–2414, May 2016.

[6] J. Kazempour, and B. F. Hobbs, "Value of flexible resources, virtual bidding, and self-scheduling in two-settlement electricity markets with wind generation-Part I: Principles and competitive model," *IEEE Trans. Power Syst.*, vol. 33, no. 1, pp. 749-759, Jan. 2018.

[7] G. Zhang, E. Ela, and Qin Wang, "Market scheduling and pricing for primary and secondary frequency reserve," *IEEE Trans. Power Syst.*, vol. 34, no. 4, pp. 2914-2924, Jul. 2019.

[8] Generation Retirement Scenario: Special Reliability Assessment, NERC, Dec. 2018.

[9] Report on the FERC-NERC-Regional Entity Joint Review of Restoration and Recovery Plans, Staffs of the FERC and the NERC and its RE, Jan. 2016.

[10] Grid Resilience in Regional Transmission Organizations and Independent System Operators, Docket No. AD18-7-000, FERC, Feb. 2018.

[11] Y. R. Rodrigues, M. M. A. Abdelaziz, and L. Wang, "Resilience-oriented D-PMU based frequency controller for islanded microgrids with flexible resources Support," *IEEE Trans. Power Del.*, Dec. 2020 (Early Access).

[12] K. P. Schneider, F. K. Tuffner, M. A. Elizondo, C.-C. Liu, Y. Xu, and D. Ton, "Evaluating the feasibility to use microgrids as a resiliency resource," *IEEE Trans. Smart Grid*, vol. 8, no. 2, pp. 687-696, Mar. 2017.

[13] L. Che, and M. Shahidehpour, "Adaptive formation of microgrids with mobile emergency resources for critical service restoration in extreme conditions," *IEEE Trans. Power Syst.*, vol. 34, no. 1, pp. 742-753, Jan. 2019.

[14] S. Lei, J. Wang, C. Chen, and Y. Hou, ''Mobile emergency generator pre-positioning and real-time allocation for resilient response to natural disasters,'' *IEEE Trans. Smart Grid*, vol. 9, no. 3, pp. 2030–2041, May 2018.

[15] S. Yao, P. Wang, and T. Zhao, "Transportable energy storage for more resilient distribution systems with multiple microgrids," *IEEE Trans. Smart Grid*, vol. 10, no. 3, pp. 3331–3341, May 2019.

[16] IEEE Std. 1547-2018, IEEE Standard for Interconnection and Interoperability of Distributed Energy Resources with Associated Electric Power Systems Interfaces. IEEE, 2018.

[17] N. Ganganath, J. V. Wang, X. Xu, C.-T Cheng, and C. K. Tse, "Agglomerative clustering based network partitioning for parallel power system restoration," *IEEE Trans. Ind. Informat.*, vol. 14, no. 8, pp. 3325-3333, Aug. 2018.

[18] T. Jiang, L. Bai, H. Jia, and F. Li, "Spectral clustering-based partitioning of volt/VAR control areas in bulk power systems," *IET Gener., Transmiss. Distrib.*, vol. 11, no. 5, pp. 1126-1133, Mar. 2017.

[19] H. Mehrjerdi, S. Lefebvre, M. Saad, and D. Asber, "A decentralized control of partitioned power networks for voltage regulation and prevention against disturbance propagation," *IEEE Trans. Power Syst.*, vol. 28, no. 2, pp. 1461-1469, May 2013.

[20] M. D. Amadou, H. Mehrjerdi, S. Lefebvre, M. Saad, and D. Asber, "Area voltage control analysis in transmission systems based on clustering technique," *IET Gener., Transmiss. Distrib.*, vol. 8, no. 12, pp. 2134-2143, May 2014.

[21] S. M. P.-Londoño, G. O.-Tost, and J. J. M.-Florez, "Online determination of voltage stability weak areas for situational awareness improvement," *Electr. Power Syst. Res.*, vol. 145, pp. 112-121, Apr. 2017.

[22] E. C.-Sanchez, P. H. D. Hines, C. Barrows, S. Blumsack, and M. Patel, "Multi-attribute partitioning of power networks based on electrical distance," *IEEE Trans. Power Syst.*, vol. 28, no. 4, pp. 4979-4987, Nov. 2013.

[23] IEEE Std 2030.8, IEEE Standard for the Testing of Microgrid Controllers, IEEE, 2018.

[24] IEEE Std 2030.8, IEEE Recommended Practice for the Planning and Design of the Microgrid, IEEE, Jul. 2019.

[25] Y. Khayat, Q. Shafiee, R. Heydari, M. Naderi, T. Dragičević, J. W. S.-Porco, F. Dörfler, M. Fathi, F. Blaabjerg, J. M. Guerrero, and H. Bevrani, "On the secondary control architectures of AC microgrids: an overview," *IEEE Trans. Power Electron.*, vol. 35, no. 6, pp. 6482-6500, Jun. 2020.

[26] M. N. Alam, S. Chakrabarti, and A. Ghosh, "Networked microgrids: state-of-the-art and future perspectives," *IEEE Trans. Ind. Informat.*, vol. 15, no. 3, pp. 1238-1250, Mar. 2019.

[27] Y. Li, P. Zhang, and P. B. Luh, "Formal analysis of networked microgrids dynamics," *IEEE Trans. Power Syst.*, vol. 33, no. 3, pp. 3418-3427, May 2018.

[28] H. Farzin, M. F.-Firuzabad, and M. M.-Aghtaie, "Role of outage management strategy in reliability performance of multi-microgrid distribution systems," *IEEE Trans. Power Syst.*, vol. 33, no. 3, pp. 2359-2369, May 2018.

[29] K. Rahbar, C. C. Chai, and R. Zhang, "Energy cooperation optimization in microgrids with renewable energy integration," *IEEE Trans. Smart Grid*, vol. 9, no. 2, pp. 1482-1493, Mar. 2018.

[30] M. Shahidehpour, Z. Li, S. Bahramirad, Z. Li, and W. Tian, "Networked microgrids: Exploring the possibilities of the IIT-Bronzeville grid," *IEEE Power Energy Mag.*, vol. 15, no. 4, pp. 63-71, Jul. 2017.

[31] A. C. Zambroni de Souza, C. A. Cañizares, and V. H. Quintana, "New techniques to speed up voltage collapse computations using tangent vectors," *IEEE Trans. Power Syst.*, vol. 12, no. 3, pp.1380-1387, Aug. 1997.

[32] Y. Jia, and Z. Xu., "A direct solution to biobjective partitioning problem in electric power networks," *IEEE Trans. Power Syst.*, vol. 32, no. 3, pp. 2481-2483, May 2017.

[33] F. Raak, Y. Susuki, and T. Hikihara, "Data-driven partitioning of power networks via Koopman mode analysis," *IEEE Trans. Power Syst.*, vol. 31, no. 4, pp. 2799-2808, Jul. 2016.

[34] I. Kamwa, A. K. Pradhan, and G. Joos, "Automatic segmentation of large power systems into fuzzy coherent areas for dynamic vulnerability assessment," *IEEE Trans. Power Syst*, vol 22(4):1974-85, Nov. 2007.

[35] I. Kamwa, A. K. Pradhan, G. Joos, and R. Samantaray, "Fuzzy partitioning of a real power system for dynamic vulnerability assessment," *IEEE Trans. Power Syst.*, vol. 24, no. 3, pp. 1356-1365, Aug. 2009.

[36] H. D. Nguyen, K. Dvijotham, and K. Turitsy, "Constructing convex inner approximations of steady-state security regions," *IEEE Trans. Power Syst.*, vol. 34, no. 1, pp. 257-267, Jan. 2019.

[37] T. Ding, R. Bo, H. Sun, F. Li, and Q. Guo, "A robust two-level coordinated static voltage security region for centrally integrated wind farms," *IEEE Trans. Smart Grid*, vol. 7, no. 1, pp. 460-470, Jan. 2016.

[38] F. F. Wu, and S. Kumagai, "Steady-state security regions of power systems," *IEEE Trans. Circuits Syst.*, vol. 29, no.11, Nov. 703-711, 1982.

[39] F. F. Wu, Y-K Tsai, Y-X Yu, "Probabilistic steady-state and dynamic security assessment," *IEEE Trans. Power Syst.*, vol. 3, no. 1, pp. 1-9, Feb. 1988.

[40] C-C. Liu, "A new method for the construction of maximal steady-state security regions of power systems," *IEEE Trans. Power Syst.*, vol. 1, no. 4, pp. 19-26, Nov. 1986.

[41] J. Z. Zhu, R. Fan, G. Xu, and C. S. Chang, "Construction of maximal steady-state security regions of power systems using optimization method," *Electr. Power Syst. Res.*, vol. 44, no. 2, pp. 101-105, Feb. 1998.

[42] H. Sharifzadeh, N. Amjady, and H. Zareipour, "Multi-period stochastic security-constrained OPF considering the uncertainty sources of wind power, load demand and equipment unavailability," *Electr. Power Syst. Res.*, 2017, vol. 146, pp. 33-42, May 2017.

[43] S. J. Chen, Q. X. Chen, Q. Xia, and C. Q. Kang, "Steady-state security assessment method based on distance to security region boundaries," *IET Gener., Transmiss. Distrib.*, vol. 7, no. 3, pp. 288-297, Dec. 2013.

[44] W. D. Oliveira, J. P. A. Vieira, U. H. Bezerra, D. A. Martins, and B. G. Rodrigues, "Power system security assessment for multiple contingencies using multiway decision tree," *Electr. Power Syst. Res.*, vol. 148, pp. 264-272, Jul. 2017.

[45] T. Van Cutsem, and C. Vournas, "Voltage stability of electric power systems," *Springer*, Boston, 1998.

[46] P. Kessel, and H. Glavitsch, "Estimating the voltage stability of a power system," *IEEE Trans. Power Del.*, vol. 1, no. 3, pp. 346-354, Jul. 1986.

[47] P. Sauer, and M. A. Pai, "Power system steady-state stability and the load-flow Jacobian," *IEEE Trans. Power Syst.*, vol. 5, no. 4, pp.1374-1383, Nov. 1990.

[48] M. Moghavvemi, and O. Faruque, "Real-time contingency evaluation and ranking technique," *IEE Proc. Gener. Transm. Distrib.*, vol. 145, no. 5, pp. 517-524, Nov. 1998.

[49] W. P. J. Philippe, S. Eftekharnejad, and P. K. Ghosh, "Development of a new voltage stability index and its implementation considering voltage, measurement uncertainty," *IET Gener. Transm. Distrib.*, vol. 13, no. 18, pp. 4011- 4020, Sep. 2019.

[50] M. Kamel, A. A. Karrar, and A. H. Eltom, "Development and application of a new voltage stability index for on-line monitoring and shedding," *IEEE Trans. Power Syst.*, vol. 33, no. 2, pp.1231-1241, Mar. 2018.

[51] Z. Liu, A. Clark, P. Lee, L. Bushnell, D. Kirschen, and R. Poovendran, "Submodular optimization for voltage control," *IEEE Trans. Power Syst.*, vol. 33, no. 1, pp. 502-513, Jan. 2018.

[52] S. C. Chevalier, and P. D. Hines, "Mitigating the risk of voltage collapse using statistical measures from PMU data," *IEEE Trans. Power Syst.*, vol. 34, no. 1, pp. 120-128, Jan. 2019.

[53] C. A. Cañizares, and Z. T. Faur, "Analysis of SVC and TCSC controllers in voltage collapse," *IEEE Trans. Power Syst.*, vol. 14, no. 1, Feb. 158-165.

[54] S. Gerbex, R. Cherkaoui, and A. J. Germond, "Optimal location of multi-type FACTS devices in a power system by means of genetic algorithms," vol. 16, no. 3, pp. 537-544, Aug. 2001.

[55] X. Huang, G. Zhang, and L. Xiao, "Optimal location of SMES for improving power system voltage stability," *IEEE Trans. Appl. Supercond.*, vol. 20, no. 3, pp. 1316-1319, Jun. 2010.

[56] Y. Xu, Z. Y. Dong, C. Xiao, R. Zhang, and K. P. Wong, "Optimal placement of static compensators for multi-objective voltage stability enhancement of power systems," *IET Gener. Transm. Distrib.*, vol. 9, no. 15, pp. 2144–2151, Nov. 2015.

[57] V. S. Kumar, K. K. Reddy, and D. Thukaram, "Coordination of reactive power in grid-connected wind farms for voltage stability enhancement," *IEEE Trans. Power Syst.*, vol. 29, no. 5, pp. 2381-2390, Sep. 2014.

[58] K. Kawabe, Y. Ota, A. Yokoyama, and K. Tanaka, "Novel dynamic voltage support capability of photovoltaic systems for improvement of short-term voltage stability in power systems," *IEEE Trans. Power Syst.*, vol. 32, no. 3, pp. 1796-1804, May 2017.

[59] O. A. Urquidez, and L. Xie, "Singular value sensitivity based optimal control of embedded VSC-HVDC for steady-state voltage stability enhancement," *IEEE Trans. Power Syst.*, vol. 31, no. 1, pp. 216-225, Jan. 2016.

[60] M. Kayikci, and J. V. Milanovic, "Reactive power control strategies for DFIG-based plants," *IEEE Trans. Ener. Conv.*, vol. 22, no. 2, pp. 389-396, Jun. 2007.

[61] Z. Lu, H. Li, and Y. Qiao, "Probabilistic flexibility evaluation for power system planning considering its association with renewable power curtailment," *IEEE Trans. Power Syst.*, vol. 33, no. 3, pp. 3285-3295, May 2018.

[62] E. H.-Forushani, M. E. H. Golshan, M. S.-Khah, P. Siano, "Optimal operation of emerging flexible resources considering sub-hourly flexible ramp product," *IEEE Trans. Sustain. Ener.*, vol. 9, no. 2, pp. 916-929, Apr. 2018.

[63] H. Hamidpour, J. Aghaei, S. Pirouzi, S. Dehghan, T. Niknam, "Flexible, reliable, and renewable power system resource expansion planning considering energy storage systems and demand response programs," *IET Renew. Power Gener.*, vol. 13, no. 11, 1862-1872, Aug. 2019.

[64] A. Jalali, M. S. Sepasian, M. K. S.-E.-Eslami, "Undisruptive load curtailment scheme to ensure voltage stability margin," *IET Gener. Transm. Distrib.*, vol. 13, no. 9, pp. 1509-1519, May 2019.

[65] A. Rabiee, A. Soroudi, B. M.-ivatloo, and M. Parniani, "Corrective voltage control scheme considering demand response and stochastic wind power," *IEEE Trans. Power Syst.*, vol. 29, no. 6, pp. 2965-2973, Nov. 2014.

[66] A. Rabiee, S. M. M.-Bonab, M. Parniani, and I. Kamwa, "Optimal cost of voltage security control using voltage dependent load models in presence of demand response," *IEEE Trans. Smart Grid*, vol. 10, no. 3, pp. 2383-2395, Jan. 2019.

[67] B. Chen, Z. Ye, C. Chen, and J. Wang, "Toward a MILP modeling framework for distribution system restoration," *IEEE Trans. Power Syst.*, vol. 34, no. 3, pp. 1749-1760, May 2019.

[68] Y. Xu, C.-C. Liu, Z. Wang, K. Mo, K. P. Schneider, F. K. Tuffner, and D. T. Ton, "DGs for service restoration to critical loads in a secondary network," *IEEE Trans. Smart Grid*, vol. 10, no. 1, pp. 435-447, Jan. 2019.

[69] S. Poudel, and A. Dubey, "Critical load restoration using distributed energy resources for resilient power distribution system," *IEEE Trans. Power Syst.*, vol. 34, no. 1, pp. 52-53, Jan. 2019.

[70] A. A. Hafez, W. A. Omran, and Y. G. Hegazy, "A decentralized technique for autonomous service restoration in active radial distribution networks," *IEEE Trans. Smart Grid*, vol. 9, no. 3, pp. 1911-1919, May 2018.

[71] W. Li, Y. Li, C. Chen, Y. Tan, Y. Cao, M. Zhang, Y. Peng, and S. Chen, "A full decentralized multi-agent service restoration for distribution network with DGs," *IEEE Trans. Smart Grid*, vol. 11, no. 2, pp. 1100-1111, Mar. 2020.

[72] B. Chen, C. Chen, J. Wang, and K. L. B.-Purry, "Sequential service restoration for unbalanced distribution systems and micro-grids," *IEEE Trans. Power Syst.*, vol. 33, no. 2, pp. 1507-1520, Mar. 2018.

[73] L. Fu, B. Liu, K. Meng, and Z. Y. Dong, "Optimal restoration of an unbalanced distribution system into multiple microgrids considering three-phase demand-side management," *IEEE Trans. Power Syst.*, vol. 36, no. 2, pp. 1350-1361, Mar. 2021.

[74] F. Shen, Q. Wu, J. Zhao, W. Wei, N. D. Hatziargyriou, and F. Liu, "Distributed risk-limiting load restoration in unbalanced distribution systems with networked microgrids," *IEEE Trans. Smart Grid*, vol. 11, no. 6, pp. 4574-4586, Nov. 2020.

[75] Arizona-Southern California Outages on September 8, 2011, Staffs of the FERC and NERC, Apr. 2012.

[76] Z. Qin, Y. Hou, C.-C., S. Liu, and W. Sun, "Coordinating generation and load pickup during load restoration with discrete load increments and reserve constraints," *IET Gener., Transm., Distrib.*, vol. 9, no. 15, pp. 2437-2446, Jul. 2015.

[77] R. R. Nejad, and W. Sun, "Distributed load restoration in unbalanced active distribution systems," *IEEE Trans. Smart Grid*, vol. 10, no. 5, pp. 5759-5769, Sep. 2019.

[78] R. R. Nejad, W. Sun, and A. Golshani, "Distributed restoration for integrated transmission and distribution systems with DERs," *IEEE Trans. Power Syst.*, vol. 34, no. 6, pp. 4964-4973, Nov. 2019.

[79] J. Zhao, H. Wang, Y. Liu, Q. Wu, Z. Wang, and Y. Liu, "Coordinated restoration of transmission and distribution system using decentralized scheme," *IEEE Trans. Power Syst.*, vol. 34, no. 5, pp. 3428-3442, Sep. 2019.

[80] J. Zhao, H. Hong, Y. Hou, Q. Wu, N. D. Hatziargyriou, W. Zhang, and Y. Liu, "Robust distributed coordination of parallel restored subsystems in wind power penetrated transmission system," *IEEE Trans. Power Syst.*, vol. 35, no. 4, Jul. 2020.

[81] J. Zhao, Q. Zhang, Z. Liu, and X. Wu, "A distributed black-start optimization method for global transmission and distribution network," *IEEE Trans. Power Syst.*, Feb. 2021 (Early Access).

[82] P. Gomes, A. C. S. de Lima, A. P. Guarani, "Guidelines for power system restoration in the Brazilian system," *IEEE Trans. Power Syst.*, vol. 19, no. 2, pp. 1159-1165, May 2004.

[83] Network Procedures, Submodule 10.11: Recompositing of the operation network after disturbance, ONS, Dez. 2016.

[84] Network Procedures, Submodule 21: Operation network recompositing after disturbance, Module 21: Studies to reinforce electrical operational safety, systemic control and facilities integration, Submodule 21.6: System restoration studies ONS, Dez. 2016.

[85] T. J. Overbye, R. P. Klump, "Effective calculation of power system low-voltage solutions," *IEEE Trans. Power Syst.*, vol. 11, no. 1, pp. 75-82, Feb. 1996.

[86] T. J. Overbye, and C. L. Marco, "Voltage security enhancement using energy based sensitivities," *IEEE Trans. Power Syst.*, vol. 6, no. 3, pp.1196-1202, Aug. 1991.

[87] C. L. Marco, T. J. Overbye, "An energy based security measure for assessing vulnerability to voltage collapse," *IEEE Trans. Power Syst.*, vol. 5, no. 2, pp. 419-427, May 1990.

[88] E. V. Lorenci, A. C. Zambroni de Souza, B. I. L. Lopes, "Energy function applied to voltage stability studies - Discussion on low voltage solutions with the help of tangent vector," *Electr. Power Syst. Res.*, vol. 41, pp. 290-299, Dec. 2016.

[89] E. V. Lorenci. Energy function applied to voltage stability studies and definition of the vulnerability profile of an electrical power system. Thesis (Doctorate in Electrical Engineering), Federal University of Itajuba, Itajubá, 2017.

[90] F. C. B. Almeida, J. A. Passos Filho, J. L. R. Pereira, A. L. M. Marcato, and E. J. Oliveira, "Assessment of the generator remote voltage control through static security regions," in *Proc. IEEE PES Gen. Meeting*, Detroit, MI, USA, 2011, pp 1-7.

[91] Network Procedures, Submodule 18.2: List of Computational Systems and Models, ONS, Dez. 2016.

[92] Organon Technical Manual, High Performance Power Systems Applications, HPPA.

[93] W. Rosehart, C. A. Canizares, and V. H. Quintana, "Effect of detailed power system models in traditional and voltage stability constrained optimal power flow problems," *IEEE Power Eng. Rev.*, vol. 22, no. 12, Feb. 2002.

[94] W. Rosehart, C. Canizares, and V. Quintana, "Optimal power flow incorporating voltage collapse constraints," in *Proc. IEEE PES Summer Meeting*, Edmonton, AB, Canada, 1999, pp. 820-825.

[95] W. D. Rosehart, C. A. Canizares and V. H. Quintana, "Multi objective optimal power flows to evaluate voltage security costs in power networks," *IEEE Trans. Power Syst.*, vol. 18, no. 2, pp. 578-587, May 2003.

[96] F. Alvarado, I. Dobson, and Y. Hu, "Computation of closest bifurcations in power systems," *IEEE Trans. Power Syst.*, vol. 9, no. 2, pp. 918-928, May 1994.

[97] G. Chen, D. J. Hill, and X. Yu, Bifurcation Control, Theory and Applications, *Springer*, Berlin, 2003.

[98] M. M. A. Abdelaziz, and E. F. El-Saadany, "Determination of worst case loading margin of droop-controlled islanded microgrids," in *Int. Conf. Electric Power and Ener. Conv. Syst.*, Istanbul, Turkey, 2013, pp. 1-6.

[99] F. W. Mohn, A. C. Z. de Souza, "Tracing PV and QV curves with the help of a CRIC continuation method," *IEEE Trans. Power Syst.*, vol. 21, no. 3, pp. 1115–1122, Aug. 2006.

[100] Balancing and Frequency Control, NERC Resources Subcommittee, Jan. 2011.

[101] Automatic Underfrequency Load Shedding, NERC Standard PRC-006-1, Nov. 2010.

[102] 2020 Frequency Response Annual Analysis, NERC Standards and Engineering Organization, Nov. 2020.

[103] I. Egido, F. F.-Bernal, P. Centeno, and L. Rouco, "Maximum frequency deviation calculation in small isolated power systems," *IEEE Trans. Power Syst.*, vol. 24, no. 4, pp. 1731-1738, Nov. 2009.

[104] Securing Wide Area Measurement Systems, Pacific Northwest National Laboratory, PNNL-17116, 2007.

[105] IEEE/IEC Std 60255-118-1-2018, IEEE/IEC International Standard for Measuring relays and protection equipment-Part 118-1: Synchrophasor for power systems, IEEE/IEC International Standard, IEEE/IEC, 2018.

[106] IEEE Std. C37.1-2007, IEEE Standard for SCADA and Automation Systems, IEEE, 2008.

[107] H.-Y. Su, Kang F.-M. Kang, and C. W. Liu, "Transmission grid secondary voltage control method using PMU data," *IEEE Trans. Smart Grid*, vol. 9, no. 4, pp. 2908-2917, Jul. 2018.

[108] M. M. Eissa, "A new wide-area protection scheme for single- and double-circuit lines using 3-D-phase surface," *IEEE Trans. Power Del.*, vol. 33, no. 6, pp. 2613-2623, Dec. 2018.

[109] M. K. Neyestanaki, and A. M. Ranjbar, "An adaptive PMU-based wide area backup protection scheme for power transmission lines," *IEEE Trans. Smart Grid*, vol. 6, no. 3, pp.1550-1559, May 2015.

[110] S. S. M.-Seyedi, F. Aminifar, and S. Afsharnia, "Application of WAMS and SCADA data to online modeling of series-compensated transmission lines," *IEEE Trans. Smart Grid*, vol. 8, no. 4, pp. 1968-1976, Jul. 2017.

[111] S. A. N. Sarmadi, A. S. Dobakhshari, S. Azizi, and A. M. Ranjbar, "A sectionalizing method in power system restoration based on WAMS," *IEEE Trans. Smart Grid*, vol. 2, no. 1, pp. 190-197, Mar. 2011.

[112] U. Rudez, and R. Mihalic, "WAMS-based underfrequency load shedding with short-term frequency prediction," *IEEE Trans. Power Del.*, vol. 31, no. 4, pp.1912-1920, Aug. 2016.

[113] Y. V. Makarov, P. Du, S. Lu, T. B. Nguyen, X. Guo, J. W. Burns, J. F. Gronquist, and M. A. Pai, "PMU-based wide-area security assessment: concept, method, and implementation," *IEEE Trans. Smart Grid*, vol. 3, no. 3, pp. 1325-1332, Sep. 2012.

[114] S. Arora, and J. W. Taylor, "Short-term forecasting of anomalous load using rule-based triple seasonal methods," *IEEE Trans. Power Syst.*, vol. 28, no. 3, pp. 3235-3242, Aug. 2013.

[115] Network Procedures, Submodule 11.8: Synchrophasor Measurement System, ONS, Dez 2016.

[116] L. Lugnani, D. Dotta, J. M. F. Ferreira, I. C. Decker, and J. H. Chow, "Frequency response estimation following large disturbances using synchrophasors," in *Proc. IEEE PES Gen. Meeting*, Portland, OR, USA, 2018, pp 1-5.

[117] C. A. S. Neto, M. A. Quadros, M. G. Santos, J. Jardim, "Brazilian System Operator online security assessment system," in *Proc. IEEE PES Gen. Meeting*, Providence, RI, USA, 2010, pp 1-7.

[118] IEEE 118-bus system, [Online]. Available in: https://labs.ece.uw.edu/pstca/pf118/ pg_tca118bus.htm. Accessed on: Jun. 08, 2021.

[119] B. P. Bhattarai, I. C. Mendaza, K. S. Myers, B. B.-Jensen, and S. Paudyal, "Optimum aggregation and control of spatially distributed flexible resources in smart grid," *IEEE Trans. Smart Grid*, vol. 9, no. 5, pp. 5311-5322, Sep. 2018.

[120] A. Akrami, M. Doostizadeh, and F. Aminifar, "Power system flexibility: an overview of emergence to evolution," *J. Mod. Power Syst. Clean Energy*, vol. 7, no. 5, pp. 987-1007, Sep. 2019.

[121] IEA-PVPS Task 14, Flexible resources for flexible transmission system operation, *Int. Ener. Agency Photovoltaic Power Syst. Programme*, Milan, October 2017.

[122] A. M.-Rad, V. W. S. Wong, J. Jatskevich, R. Schober and A. L.-Garcia, "Autonomous demand-side management based on game-theoretic energy consumption scheduling for the future smart grid," *IEEE Trans. Smart Grid*, vol. 1, no. 3, pp. 320-331, Dec. 2010.

[123] E. Lannoye, D. Flynn, and M. O'Malley, "Evaluation of power system flexibility," *IEEE Trans. Power Syst.*, vol. 27, no. 2, pp. 922-931, May 2012.

[124] P. Palensky, E. Widl, M. Stifter, and A. Elsheikh, "Modeling intelligent energy systems: co-simulation platform for validating flexible-demand EV charging management," *IEEE Trans. Smart Grid*, vol. 4, no. 4, pp. 1939-1947, Dec. 2013.

[125] Y. R. Rodrigues, A. C. Zambroni de Souza, and P. F. Ribeiro, "An inclusive methodology for plug-in electrical vehicle operation with G2V and V2G in smart microgrid environments," *Int. J. Electr. Power Ener. Syst.*, vol. 102, pp. 312-323, Nov. 2018.

[126] M. R. Monteiro, G. F. Alvarenga, Y. R. Rodrigues, A. C. Z. de Souza, B. I. L. Lopes, M. C. Passaro, and M. Abdelaziz, "Network partitioning in coherent areas of static voltage stability applied to security region enhancement," *Int. J. Electr. Power Ener. Syst.*, vol. 117, May 2020.

[127] E. Riccietti, S. Bellavia, and S. Sello, "Sequential linear programming and particle swarm optimization for the optimization of energy districts," Eng. Optimization, vol. 51, no. 1, pp. 84-100, Mar. 2018.

[128] R. A. Jabr, "Robust Volt/VAr control with photovoltaics," *IEEE Trans. Power Syst.*, vol. 34, no. 3, pp. 2401-2408, May 2019.

[129] H. Wang, and J. Huang, "Incentivizing energy trading for interconnected microgrids," *IEEE Trans. Smart Grid*, vol. 9, no. 4, pp. 2647-2657, Jul. 2018.

[130] C. Yuen, A. Oudalov, and A. Timbus, "The provision of frequency control reserves from multiple microgrids," *IEEE Trans. Ind. Electron.*, vol. 58, no. 1, pp. 173-183, Jan. 2011.

[131] Powering up the neighborhood grid: A strategic entry plan for the microgrid business, PWC, 2016.

[132] PJM Manual 36: System Restoration, Revision: 29, System Operations Division, Jun. 2021.

[133] IEEE 57-bus Feeder, [Online]. Available in: http://labs.ece.uw.edu/pstca/pf57 /pg_tca57bus.htm. Accessed on: Jun. 08, 2021.

[134] IEEE 123-bus Feeder, IEEE PES AMPS DSAS Test Feeder Working Group, [Online]. Available: http://sites.ieee.org/pes-testfeeders/ resources/. Accessed on: Jun. 08, 2021.

[135] IEEE 34-bus Feeder, IEEE PES AMPS DSAS Test Feeder Working Group, [Online]. Available: http://sites.ieee.org/pes-testfeeders/ resources/. Accessed on: Jun. 08, 2021.

Appendix A: Parameters for SSR Formation

The restrictions of active and reactive power are depicted in Table A.1 and the respective under- and over-voltage restriction limits are collected in the set $\left\{ \underline{V_i}, \overline{V_i} \right\} = \{0.9, 1.1\}$ (p.u.), while the angular limit is calculated by (A.1).

Table A.1: Restrictions of active and reactive power

Bus	$\underline{P_{\langle G \rangle}}$ (MW)	$\overline{P_{\langle G \rangle}}$ (MW)	$\underline{Q_{\langle G \rangle}}$ (MVar)	$\overline{Q_{\langle G \rangle}}$ (MVar)
10,80	0	508.8	-100.0	100.0
12	0	100.0	-100.0	100.0
25	0	258.8	-100.0	100.0
26	0	350.2	-100.0	250.0
31,59,85,87	0	163.2	-300.0	300.0
45,47,48, 71,75	0	400.0	-	-
46,54,103	0	163.2	-100.0	100.0
49	0	308.9	-100.0	100.0
61	0	213.2	-100.0	100.0
65	0	408.8	-100.0	100.0
66	0	463.2	-100.0	100.0
89	0	663.2	-100.0	100.0
100	0	308.8	-100.0	100.0
111	0	108.8	-100.0	200.0
118	0	363.2	-100.0	100.0

$$\overline{\theta_{ij}} \approx \overline{I_{ij}} / \left[\overline{V_i} \cdot (G_{ij} + j \cdot B_{ij}) \right] \tag{A.1}$$

where $\overline{I_{ij}}$ is the maximum current in the branch between the buses i and j, $\overline{\theta_{ij}}$ is the angle difference between them.